WRF Model Sensitivity to Land Surface Model and Cumulus Parameterization under Short-Term Climate Extremes over the Southern Great Plains of the United States

LISI PEI

State Key Laboratory of Atmospheric Boundary Layer Physics and Atmospheric Chemistry, Institute of Atmospheric Physics, Chinese Academy of Sciences, and University of Chinese Academy of Sciences, Beijing, China, and Department of Geography and Center for Global Change and Earth Observations, Michigan State University, East Lansing, Michigan

NATHAN MOORE, SHIYUAN ZHONG, AND LIFENG LUO

Department of Geography and Center for Global Change and Earth Observations, Michigan State University, East Lansing, Michigan

DAVID W. HYNDMAN

Department of Geological Sciences, Michigan State University, East Lansing, Michigan

WARREN E. HEILMAN

USDA Forest Service Northern Research Station, Lansing, Michigan

ZHIQIU GAO

State Key Laboratory of Atmospheric Boundary Layer Physics and Atmospheric Chemistry, Institute of Atmospheric Physics, Chinese Academy of Sciences, Beijing, China

(Manuscript received 1 January 2014, in final form 17 July 2014)

ABSTRACT

Extreme weather and climate events, especially short-term excessive drought and wet periods over agricultural areas, have received increased attention. The Southern Great Plains (SGP) is one of the largest agricultural regions in North America and features the underlying Ogallala-High Plains Aquifer system worth great economic value in large part due to production gains from groundwater. Climate research over the SGP is needed to better understand complex coupled climate–hydrology–socioeconomic interactions critical to the sustainability of this region, especially under extreme climate scenarios. Here the authors studied growing-season extreme conditions using the Weather Research and Forecasting (WRF) Model. The six most extreme recent years, both wet and dry, were simulated to investigate the impacts of land surface model and cumulus parameterization on the simulated hydroclimate. The results show that under short-term climate extremes, the land surface model plays a more important role modulating the land–atmosphere water budget, and thus the entire regional climate, than the cumulus parameterization under current model configurations. Between the two land surface models tested, the more sophisticated land surface model produced significantly larger wet bias in large part due to overestimation of moisture flux convergence, which is attributed mainly to an overestimation of the surface evapotranspiration during the simulated period. The deficiencies of the cumulus parameterizations resulted in the model's inability to depict the diurnal rainfall variability. Both land surface processes and cumulus parameterizations remain the most challenging parts of regional climate modeling under extreme climates over the SGP, with the former strongly affecting the precipitation amount and the latter strongly affecting the precipitation pattern.

1. Introduction

The Southern Great Plains (SGP) of the United States is a key agricultural region in North America, which has experienced numerous climate extremes including

Corresponding author address: Shiyuan Zhong, Department of Geography, Michigan State University, 673 Auditorium Rd., Rm. 116, East Lansing, MI 48824.
E-mail: zhongs@msu.edu

DOI: 10.1175/JCLI-D-14-00015.1

major droughts (Schubert et al. 2008). As a mitigation strategy, irrigation started in the 1930s with groundwater withdrawn from the underlying Ogallala-High Plains Aquifer (Kanemasu et al. 1983; McGuire 2009). The rapid growth in groundwater withdrawals has resulted in drastic declines of aquifer storage by more than 333 km^3 (McGuire 2009). Despite the rapid water table drawdown, irrigated acreage continues to expand to meet the socioeconomic demands for food and energy production (Basso et al. 2013). This trend, along with projected changes in land–atmosphere interaction, air temperature, and precipitation (Barnston and Schickedanz 1984; Moore and Rojstaczer 2001, 2002; Mahmood et al. 2006; DeAngelis et al. 2010; Qian et al. 2013) raised major concerns about the sustainability of water resources over this region.

To better understand the complex climate–hydrology–socioeconomic interactions and establish long-term policies to ensure the water sustainability over the SGP, there is a strong need for research to improve our knowledge about precipitation processes and how other components of the climate system affect precipitation and in turn the variability of the regional hydrological cycle. Over the SGP region, summer rainfall is mostly produced from convective systems that are highly affected by the moisture transport from the Gulf of Mexico (Higgins et al. 1997) as well as the linked local atmospheric instability and soil moisture conditions through land–atmosphere coupling (Lee et al. 2010). This coupling is considered to be particularly strong in the SGP region as it is located in the transition zone between dry and wet climates (Koster et al. 2004).

Among the key tools for studying the land–atmosphere interactions are regional climate models (RCMs; Dickinson et al. 1989; Leung et al. 2003; Liang et al. 2012). Compared to general circulation models (GCMs), RCMs have higher spatial resolution and are able to capture physical processes unresolvable with the coarser resolution in GCMs. However, even at a 10-km resolution, there are still small-scale processes that cannot be fully resolved by RCMs and have to be parameterized (Leung et al. 2003). Among them, convective processes and land surface processes are directly related to the land–atmosphere coupling and are key to its strength. Parameterizations of these processes are critical for RCMs and can strongly affect precipitation variability (Ruane and Roads 2008).

Various cumulus parameterization schemes have been developed for RCMs and GCMs to represent local convection in the numerical simulations (Kuo 1974; Kain and Fritsch 1993; Betts and Miller 1993; Grell 1993; Janjić 1994; Zhang and McFarlane 1995; Grell and Devenyi 2002). These schemes usually employ different trigger and closure assumptions, and are thus suitable for different convective regimes (Liang et al. 2004a,b; Mapes et al. 2004; Zhu and Liang 2007). Despite a plethora of convection schemes, precipitation events are still difficult to replicate accurately (Liang et al. 2007), especially extreme individual precipitation events that are highly sensitive to the parameterization of deep convection (Garrett and Müller 2008).

In addition to cumulus convection, physical processes at the land–atmosphere interface are also parameterized in RCMs and GCMs. With the improved knowledge of how groundwater and canopy processes can contribute to entire land surface fluxes (Dickinson et al. 1998; Fan et al. 2007; Kollet and Maxwell 2008; Emanuel et al. 2014; Leng et al. 2014; Yuan et al. 2014), land surface models are now incorporating more comprehensive physics processes (Chen and Kumar 2001; Warrach et al. 2002; Niu et al. 2005, 2007; Miguez-Macho et al. 2007; Oleson et al. 2010; Choi and Liang 2010; Niu et al. 2011; Xie et al. 2012). For example, the widely used Noah land surface model (Chen et al. 1996; Ek et al. 2003) has been augmented to become Noah Multi-Physics (Noah-MP; Niu et al. 2011; Yang et al. 2011) in the Weather Research and Forecasting (WRF) Model (Skamarock et al. 2008), with a set of parameterizations designed to improve the representations of groundwater process, canopy physics, snowpack influence, and frozen soil impacts (Niu et al. 2011).

Since both land surface processes and convection are key elements for understanding land–atmosphere interactions, the purpose of this study is to examine their relative importance in simulating regional hydroclimate and the model sensitivity to different parameterization schemes for these processes. In particular, we examine the model sensitivity under the unusually wet or dry conditions during the growing season (April–September). As extreme events like droughts and heavy precipitation have increased in frequency in the past 30 years over the Great Plains, especially in the last 15 years (Fig. 1), proper simulations of regional hydroclimate during the six most recent extremely wet (1997, 1999, and 2004) and dry (1998, 2000, and 2011) growing seasons are desired.

In WRF, a variety of cumulus parameterizations and other precipitation controls have been developed for more accurate water cycling. In this study, we will test the sensitivity of the simulated hydrologic cycle over the SGP under extremely wet and dry growing-season conditions to two widely used cumulus parameterization schemes in WRF, namely, the Grell 3D ensemble (G3D) scheme (Grell and Devenyi 2002) and the Kain–Fritsch (KF) scheme (Kain and Fritsch 1993; Kain 2004). We will also test how much the "multi-physics" improvement of Noah-MP over the original Noah affects the simulated hydroclimate over this region. By carefully comparing the simulation results with the two cumulus parameterization

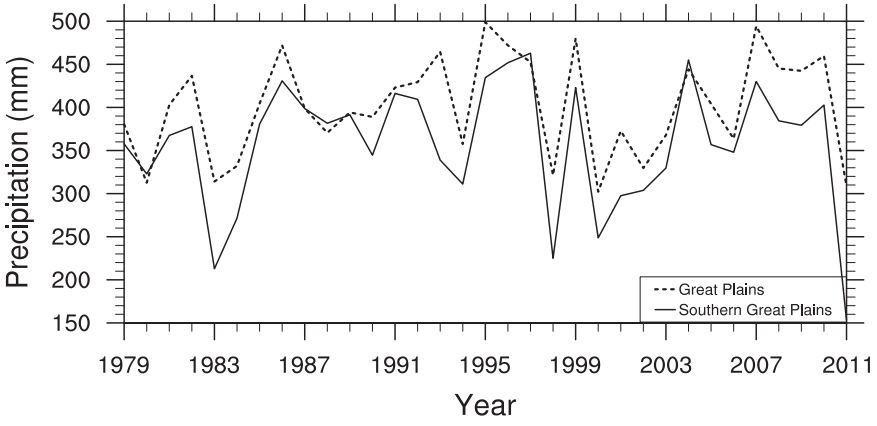

FIG. 1. Observed growing-season accumulated precipitation (mm) over the Great Plains (purple rectangle in Fig. 2) and the Southern Great Plains (SGP; blue rectangle in Fig. 2).

schemes and the two land surface models, we will address the following questions:

1) To what extent does inclusion of groundwater process and canopy physics in Noah-MP (cf. the original Noah land surface model) affect the simulated surface energy and atmospheric water balance over the SGP?
2) Based on the land surface models and cumulus parameterizations applied here, which model process—land surface or convection—has larger impacts on the simulated precipitation and other weather variables in the time scale of an entire growing season over the SGP during excessive wet and dry periods?

Section 2 describes the model configuration, experimental design, and the data used for model evaluation. Section 3 presents the simulation results and sensitivity analysis, with a focus on evaluating the simulated precipitation and atmospheric moisture budget (sections 3a–c), as well as the validation of surface latent heat flux (section 3d). Our conclusions and discussion are presented in section 4.

2. Model and data

a. Model description and experimental design

The WRF Model (version 3.4.1) is used in this study to perform all simulations. All integrations were conducted from 1 February to 30 September of each of the selected wet and dry years. The first two months of outputs were discarded as model spinup.

Our current choices of domain configuration and lateral boundary conditions were chosen based on a series of sensitivity runs with different domains and large-scale forcing fields. The current configuration (Fig. 2) consists of two two-way nested grids, with the outer grid centered at 35.16°N, 101.61°W over Amarillo, Texas, and covering most of the contiguous United States, northern Mexico, and the Gulf of Mexico and the inner grid over the SGP. The horizontal resolutions for the two grids are 27 and 9 km, respectively, with 35 vertical layers from near the surface to the model top at 100 hPa. Increasing the size of both the coarse and the fine grids and the position of the fine grid within the coarse grid did not result in significant differences in the results. Among the two large-scale forcing fields used, namely, the Climate Forecast System Reanalysis (CFSR; Saha et al. 2010) and the North American Regional Reanalysis (NARR; Mesinger et al. 2006), the CFSR dataset better resolved the topographic rainfall associated with the Rocky Mountains than the NARR in both the wet and dry years and was thus selected to provide initial and lateral boundary conditions for the WRF simulations.

For each of the six selected years, three numerical experiments were performed, representing different combinations of land surface models and cumulus parameterizations (Table 1). Except for the differences in land surface model and cumulus parameterization, all other model parameterizations are kept identical. These include the WRF single-moment 6-class microphysics scheme (WSM6; Hong and Lim 2006) for explicitly resolved rainfall, the Mellor–Yamada–Janjić (MYJ) turbulent kinetic energy scheme (Mellor and Yamada 1982; Janjić 1990, 1994, 2001) for the planetary boundary layer, and the Rapid Radiative Transfer Model (RRTM) longwave radiation scheme (Mlawer et al. 1997) and the Dudhia shortwave radiation scheme (Dudhia 1989) for the terrestrial and solar radiation processes, respectively.

b. Cumulus parameterizations

Modeling convection in this region is a challenge for many reasons including resolving the Great Plains low-level jet (Zhong et al. 1996; Weaver and Nigam 2011),

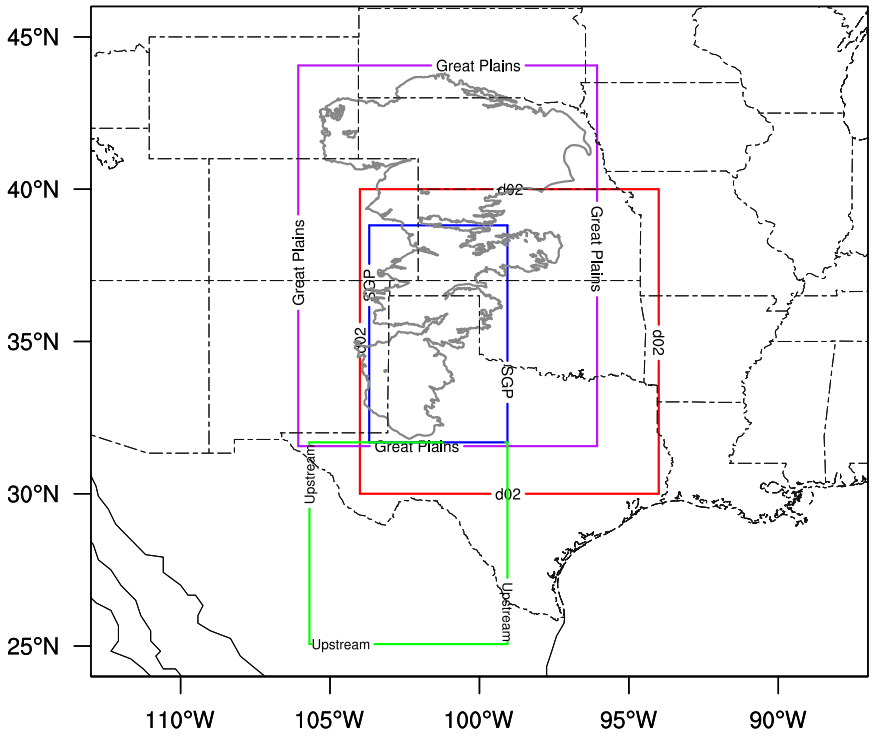

FIG. 2. Map of the study area and domain configuration. The black and red rectangles indicate the outer and inner mesh, respectively; the purple and blue rectangles outline the areas over the Great Plains and the SGP that are used for the analysis; the green rectangle denotes the upstream area; the gray polygon is the outline of the Ogallala-High Plains Aquifer.

describing the development of mesoscale convective complexes (Carbone and Tuttle 2008), and capturing dryline dynamics (Hoch and Markowski 2005). Cumulus parameterizations in numerical models are highly regime selective because they are based on fundamentally different assumptions and parameters (Liang et al. 2004a). Previous studies (Liang et al. 2004a) have shown that when convection is governed by large-scale tropospheric forcing, the Grell (1993) scheme better captures the nocturnal precipitation maximum over the Great Plains than the KF scheme (Kain and Fritsch 1993; Kain 2004). The KF scheme uses low-level vertical motion as a trigger function and the convective available potential energy removal as the closure, thus it can provides better simulations of convective processes associated with late afternoon thermodynamic vertical motion induced by heating at the lower boundary.

The SGP's summer rainfall is a combination of the late-afternoon convective precipitation and the nighttime maxima associated with large-scale synoptic forcing, mainly the development of the low-level jet. Based on the Grell (1993) framework, the G3D cumulus parameterization scheme (Grell and Devenyi 2002) employs a large ensemble of closure assumptions and parameters that are commonly used in numerical models and uses statistical techniques to determine the optimal value for feedback to the entire model. In this study, the G3D scheme and the KF scheme were used, as each is likely to better describe part of the convective regime over the SGP region. The current study also examines the relative importance of the cumulus parameterizations relative to that of the land surface model described below.

c. *Land surface models*

The Noah land surface model has been widely used by both operational weather and climate predictions and research communities (Ek et al. 2003; Hogue et al. 2005; De Haan et al. 2007; Xia et al. 2013). Problems in Noah are reported to be mainly induced by inadequate representations of the complete physical processes. These inadequacies are in the combined surface layer of vegetation and soil surface, a bulk layer of snow and soil,

TABLE 1. Description of experiments.

Expt	Cumulus parameterization	Land surface model
Noah-G3D	G3D	Noah
Noah-MP-G3D	G3D	Noah-MP
Noah-MP-KF	KF	Noah-MP

and the absence of groundwater processes (Niu et al. 2011). The Noah-MP was intended to overcome some of the shortcomings in the original Noah. The groundwater process included by Noah-MP introduced an unconfined aquifer to calculate the water exchange between the soil and groundwater, and applied a simple topography based hydrological model (TOPMODEL)-based (Beven and Kirkby 1979) runoff scheme (Niu et al. 2005, 2007) to compute surface runoff and groundwater discharge (Niu et al. 2011). In this way, the immediate removal of the water below the 2-m soil in the Noah (free gravitational drainage scheme) can be represented in the Noah-MP to allow the vertical water exchange between soil and groundwater and thus maintain a longer soil moisture memory of the antecedent weather events and climate anomalies. Also the involvement of a separate canopy model in Noah-MP has significantly improved the physical realism of the vegetated area (Yang and Friedl 2003; Niu and Yang 2004) though improvements in simulated climate response have not been well studied. In this study, we compare the performance of the Noah-MP with Noah for simulating the water cycle over the SGP during unusually wet and dry growing-season conditions.

d. Data and general analysis method

The surface variables from the three numerical experiments for each of the six years are evaluated with the forcing datasets of the North American Land Data Assimilation System project phase 2 (NLDAS-2; Cosgrove et al. 2003; Luo et al. 2003; Xia et al. 2012). Among the 11 NLDAS-2 surface forcing variables, the hourly precipitation is provided by actual observations rather than model outputs. It is a product of a temporal disaggregation of a gauge-only Climate Prediction Center analysis of daily precipitation, performed directly on the NLDAS-2 grid (0.125°) and including an orographic adjustment based on the widely applied Parameter-Elevation Regressions on Independent Slopes Model (PRISM) climatology (Cosgrove et al. 2003). In this study, the simulated precipitation and 2-m air temperature are evaluated using the NLDAS-2 forcing datasets, while the surface latent heat fluxes are evaluated using the Moderate Resolution Imaging Spectroradiometer (MODIS) satellite-derived global monthly evapotranspiration (ET) datasets (hereafter MOD16; Mu et al. 2011). The large-scale atmospheric moisture budget is validated by NARR data. Most analysis focuses on the averages across all wet and all dry years and the overall difference between the wet and dry years, while analysis of individual year(s) is conducted only when more in-depth analysis is necessary to gain insight into processes. All analysis used results from the inner grid and general statistical methods were applied.

3. Results

a. Daily precipitation

In this section, the simulated daily precipitation averaged over the SGP is evaluated relative to the observations. Figure 3 shows the growing-season time series of the observed and simulated daily precipitation averaged over the SGP. Regardless of the schemes used or wet/dry classification, all simulations adequately captured the daily and seasonal variations of the observed precipitation events. The simulated precipitation amount, however, differs substantially among the simulations and it appears to be much more sensitive to the choice of land surface model than to the cumulus parameterization scheme. Noah-MP significantly enhances precipitation, leading to a substantial wet bias especially in summer and in dry years. It is interesting to note that it more than tripled the observed value of precipitation for the exceptionally dry summer of 2011. In comparison, the simulated rainfall difference induced by changing the cumulus parameterization is relatively small. Overall, the Noah-G3D agrees best with the observations in the amount and daily to seasonal variation especially in the dry years.

To quantify the simulation skill, model errors (Table 2) are calculated and are categorized into three types: total error [RMSE, Eq. (1)], systematic error [bias, Eq. (2)] and nonsystematic error [RMSEdb, Eq. (3)] (Ruiz et al. 2010) as follows:

$$\mathrm{RMSE} = \sqrt{\frac{\sum(m_i - o_i)^2}{N}}, \tag{1}$$

$$\mathrm{bias} = \frac{\sum(m_i - o_i)}{N}, \tag{2}$$

$$\mathrm{RMSEdb} = \sqrt{\frac{\sum(m_i - o_i - \mathrm{bias})^2}{N}}, \tag{3}$$

$$R = \frac{\sum(m_i - \overline{m})(o_i - \overline{o})}{\sqrt{\sum(m_i - \overline{m})^2}\sqrt{\sum(o_i - \overline{o})^2}}, \tag{4}$$

where m_i is the spatially averaged daily precipitation from model outputs; o_i is the spatially averaged daily precipitation from observations; and N is the number of days of the growing season (183 for each year). Here R is the correlation coefficient between the temporal variations of the observed and modeled values [Eq. (4)]. The results from 1997, 1999, and 2004 are averaged to represent the wet years while those from 1998, 2000, and 2011 are averaged to represent the dry years.

For all three numerical experiments, the total error, which is dominated by nonsystematic errors, is larger for

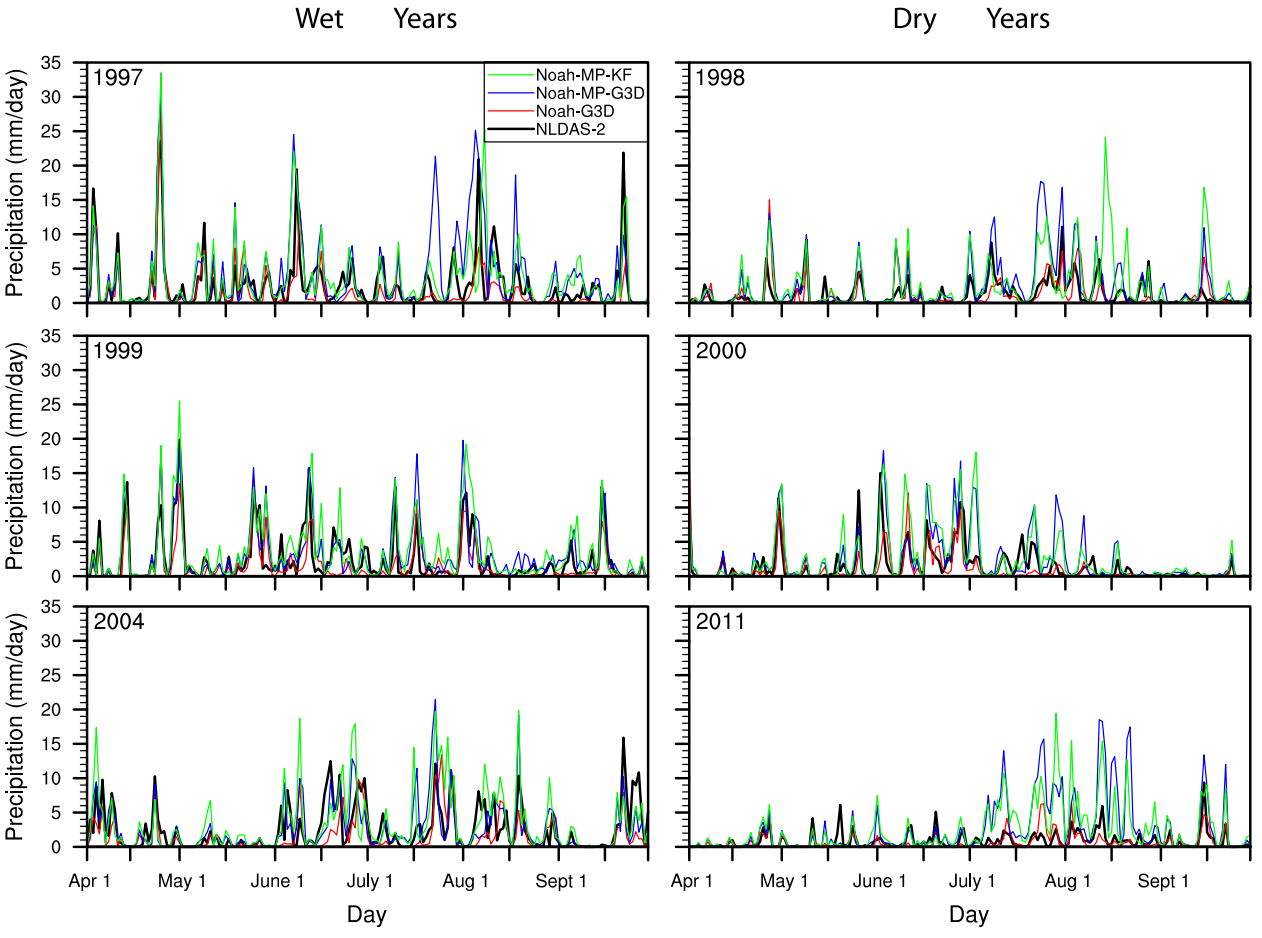

FIG. 3. Observed and simulated daily precipitation (mm day^{-1}) over the SGP from 1997–2000, 2004, and 2011.

the wet years compared to the dry years (Table 2). Noah-G3D has the smallest total error for both wet and dry scenarios; the total errors in the other two experiments are comparable. The systematic error, which represents mean bias in the simulation, is relatively small and positive (wet bias) for Noah-MP-based simulations while smaller and negative (dry bias) for Noah-G3D. The larger total error in wet years highlights the difficulties in replicating increased moisture transport and convection in the simulations. The differences corresponding to different land surface models are more significant than those associated with different cumulus parameterizations.

Previous studies have shown that climate models may generate fairly realistic mean precipitation, resulting from the wet biases for light precipitation and dry biases for heavy precipitation cancelling each other (DeAngelis et al. 2013). To better understand the biases under different rainfall categories, we separate the domain-averaged daily precipitation into five categories of 0–1, 1–3, 3–5, 5–10, and >10 (mm day^{-1}), referring to the clear day, small rainfall events, median rainfall events, heavy rainfall episodes, and extreme rainfall events, respectively. Figure 4 shows the mean, maximum (overestimation), and minimum (underestimation) biases in each category by

TABLE 2. Statistics for spatially averaged growing-season daily precipitation (mm day^{-1}).

	Total error		Systematic error		Nonsystematic error		R	
Expt	Wet	Dry	Wet	Dry	Wet	Dry	Wet	Dry
Noah-G3D	2.75	1.63	−0.91	−0.28	2.60	1.60	0.69	0.61
Noah-MP-G3D	3.36	3.21	0.76	1.28	3.25	2.94	0.69	0.65
Noah-MP-KF	3.58	3.35	1.00	1.36	3.43	3.05	0.66	0.55

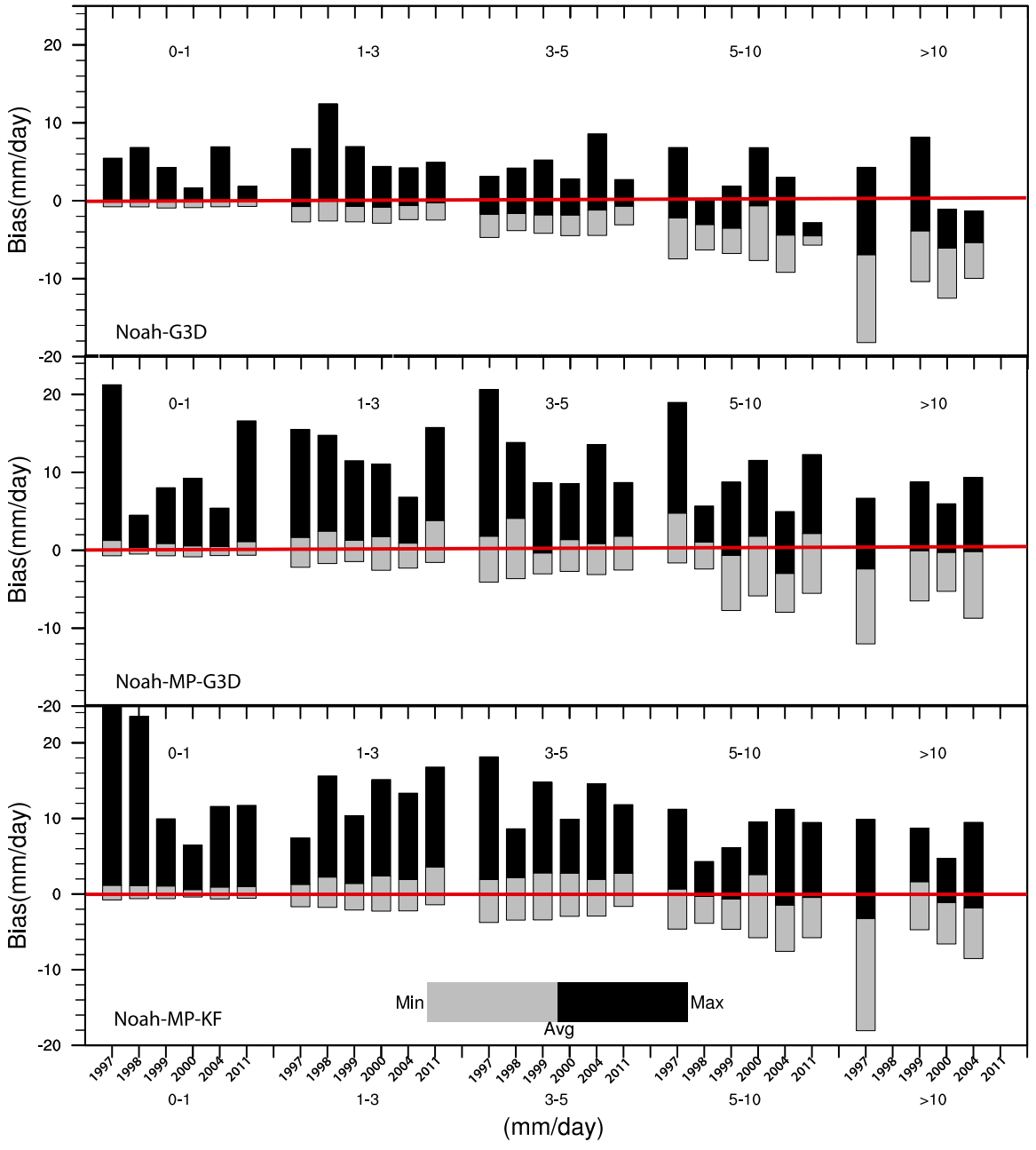

FIG. 4. Categorized daily precipitation bias over SGP for (top to bottom) Noah-G3D, Noah-MP-G3D, and Noah-MP-KF. The five categories (0–1, 1–3, 3–5, 5–10, and >10 mm day^{-1}) are defined by observations.

the three experiments. Consistent with the above statistics, the Noah-G3D has dry mean biases overall, especially for more intense rainfall, while the other two have relatively stable wet mean biases in all categories. The maximum and minimum biases reveal the model's uncertainty in simulating individual daily precipitation events over this region through the entire growing season. With Noah-G3D, these biases are about 50% less than those of the other two in all categories, and significantly smaller in the 0–1 mm day^{-1} events, both in dry and wet years. The shift from higher wet bias in light precipitation to higher dry bias in heavy precipitation is common in many modeling studies (Iorio et al. 2004; Emori et al. 2005; Kimoto et al. 2005; Kharin et al. 2007; Perkins et al. 2007; Sun et al. 2007; Wehner et al. 2010). This feature is clear here in Noah-G3D, while the other two show consistent wet biases throughout all categories. In general, the discrepancies between Noah and Noah-MP are more significant than

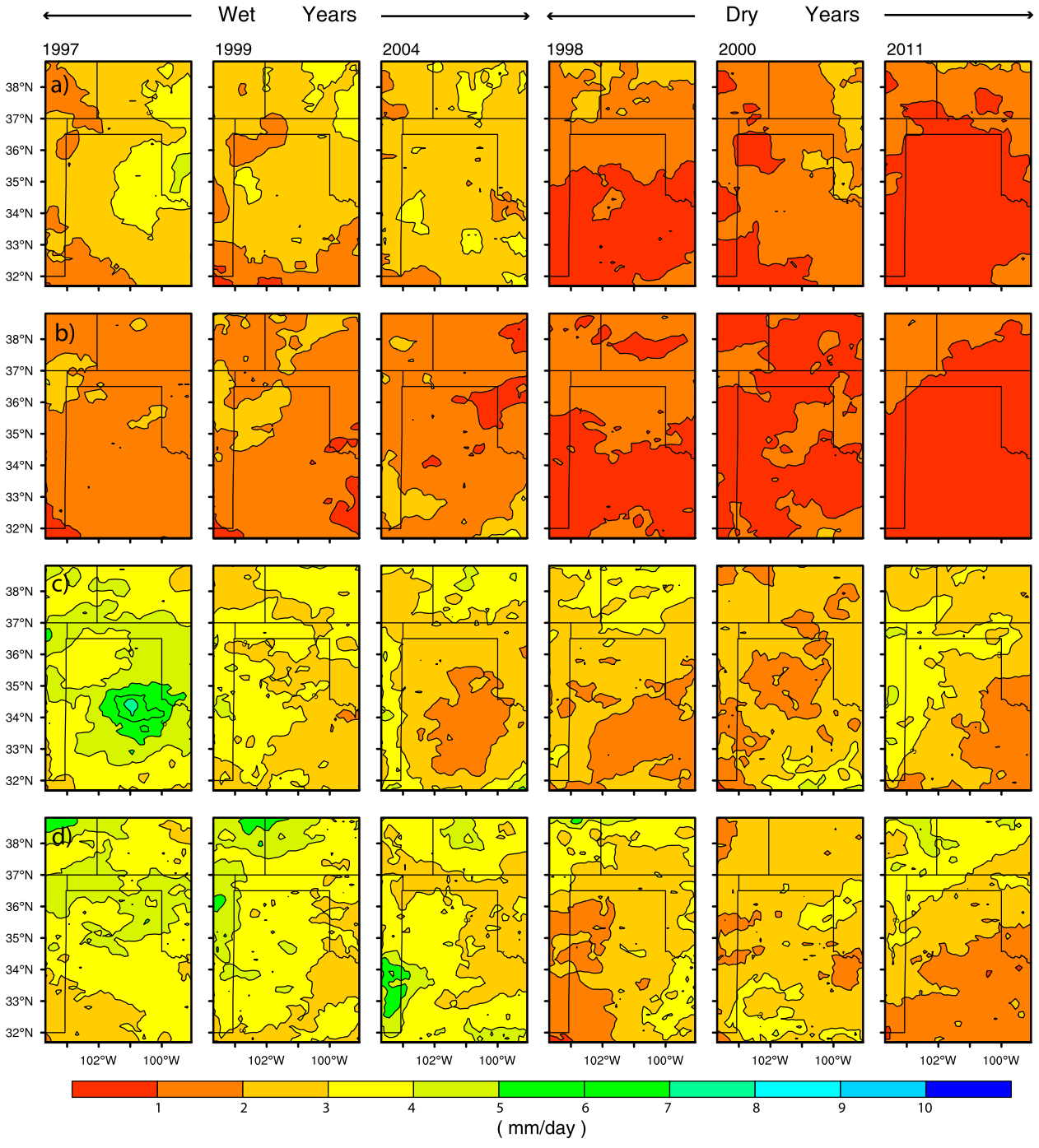

FIG. 5. Spatial distribution of the growing-season mean daily precipitation (mm day^{-1}) by (top)–(bottom) (a) observations, (b) Noah-G3D, (c) Noah-MP-G3D, and (d) Noah-MP-KF and (left)–(right) wet years (1997, 1999, and 2004) and dry years (1998, 2000, and 2011).

those between Noah-MP-G3D and Noah-MP-KF. A percentiles box plot (not shown) of the spatially averaged daily rainfall biases further demonstrates that besides the general overestimation by Noah-MP-G3D and Noah-MP-KF and underestimation by Noah-G3D, more biases are produced in wet years than dry years.

Figure 5 shows the spatial distribution of the growing-season mean daily precipitation from the three experiments and observations in all six years. Replacing Noah by Noah-MP yields significant wet biases across the study domain, and the Noah-G3D produces the best spatial distributions for dry years. Updating the land surface

TABLE 3. Centered pattern correlation coefficients between the observed and the simulated pattern of growing-season mean daily precipitation for the three experiments at each of the six years.

	Noah-G3D	Noah-MP-G3D	Noah-MP-KF
1997	0.25	0.53	0.18
1999	0.33	0.20	0.27
2004	0.06	0.15	0.26
Wet-year average	**0.21**	**0.29**	**0.24**
1998	0.61	0.78	0.55
2000	0.19	0.01	0.03
2011	0.74	0.18	0.73
Dry-year average	**0.51**	**0.32**	**0.44**

model from Noah to Noah-MP affects the simulated precipitation amount more than the spatial distribution, while the use of the two cumulus schemes leads to larger changes in spatial pattern than the amount. The centered pattern correlation coefficients (anomalies from a central mean) of mean daily precipitation are listed in Table 3. The dry-year simulations, in general, have a higher pattern correlation than that of the wet years. While Noah-G3D produces better agreement with the observed precipitation amounts in both dry and wet years (Table 2) and higher spatial correlation in dry years, Noah-MP has higher spatial correlation with the observed pattern in wet years.

b. *Atmospheric moisture flux*

Moisture availability is an important factor for rainfall amount, especially for a region like the SGP that relies heavily on the remote moisture source from the Gulf of Mexico (Higgins et al. 1997; Whiteman et al. 1997). To help understand the differences in the simulated precipitation over the SGP, this section examines how well the simulations capture moisture transport into and out of the SGP region. The growing-season averages of horizontal moisture fluxes across the four lateral boundaries boarding SGP are calculated by averaging hourly model outputs in wet and dry years from the three simulations. These simulated moisture fluxes are then compared with the observed fluxes that are estimated using NARR data averaged over the 3-h interval for the entire growing season. The results of the comparisons are shown in Figs. 6 and 7 for wet and dry years, respectively, and the corresponding vertically integrated moisture flux values at the four lateral boundaries are listed in Tables 4 and 5. Since the elevations of the SGP range from 300 to 1000 m from the east to the west, with the majority over 750 m, our analysis of the moisture transport starts from 950 hPa.

As shown in Figs. 6 and 7, the spatial patterns of the moisture flux at all four boundaries are well simulated both in wet and dry years compared to NARR. The patterns are also very similar between dry and wet years, although the magnitudes differ. In both wet and dry years, a significant amount of moisture influx to the region is found at the southern boundary in the lower troposphere below 850 hPa, most of which can be attributed to the transport of moisture from the Gulf of Mexico by the Great Plains low-level jet (identified with 850-hPa wind fields, not shown). All three experiments reasonably capture this southerly influx in both wet and dry years, with slight overestimation in the amount (Table 4).

More moisture influx between 950 and 850 hPa at the eastern and southern boundary is found in NARR during wet years compared to dry years (Figs. 6a and 7a). This feature is well captured by Noah-MP-based simulations. Noah-G3D underestimated the entrainment at the lower eastern boundary (Figs. 6 and 7, east, blue shaded area) possibly due to less simulated convective rainfall over the entire SGP compared to Noah-MP (not shown). The Rockies prohibit most of the direct moisture transfer to the SGP from the west in the lower boundary. By acting as an elevated heating source, the Rockies may prompt, under weak synoptic forcing, the development of a daytime mountain–plain circulation that drives subsidence over the SGP and outflow toward the foothills to the west of the SGP (Ruane 2010). This outflow is stronger in wet years than dry years as revealed by NARR, and has been well represented by all simulations (Figs. 6 and 7, west). In the lower boundary layer (below 850 hPa) during wet years, the Noah-MP-G3D has the least bias in SGP net moisture flux with only a slight overestimation, while Noah-G3D has the least bias in dry years with a slight underestimation (Table 4). This tendency of moisture biases coincides with the mean bias (systematic error) of the simulated spatially averaged daily precipitation discussed above (Table 2).

From 850 to 700 hPa, the moisture transferred into the SGP from the west is enhanced to about 50% of that from the south in the NARR reanalysis (Table 5), representing the secondary moisture source at this layer. This westerly moisture influx above the boundary layer is represented by all experiments in both wet and dry years, but with 20%–50% overestimation. The biases in the simulated southerly moisture transport are larger in this layer than in the layer below 850 hPa, with Noah-G3D underestimating by 10% (dry) to 14% (wet) and Noah-MP overestimating 15% (wet) to 24% (dry) compared to NARR. Discrepancies in the simulated moisture source between the three experiments are also much larger than that in the lower boundary layer.

In general, the simulated atmospheric moisture fluxes into and out of the SGP are evidently sensitive to the choice of land surface model and cumulus parameterization, with

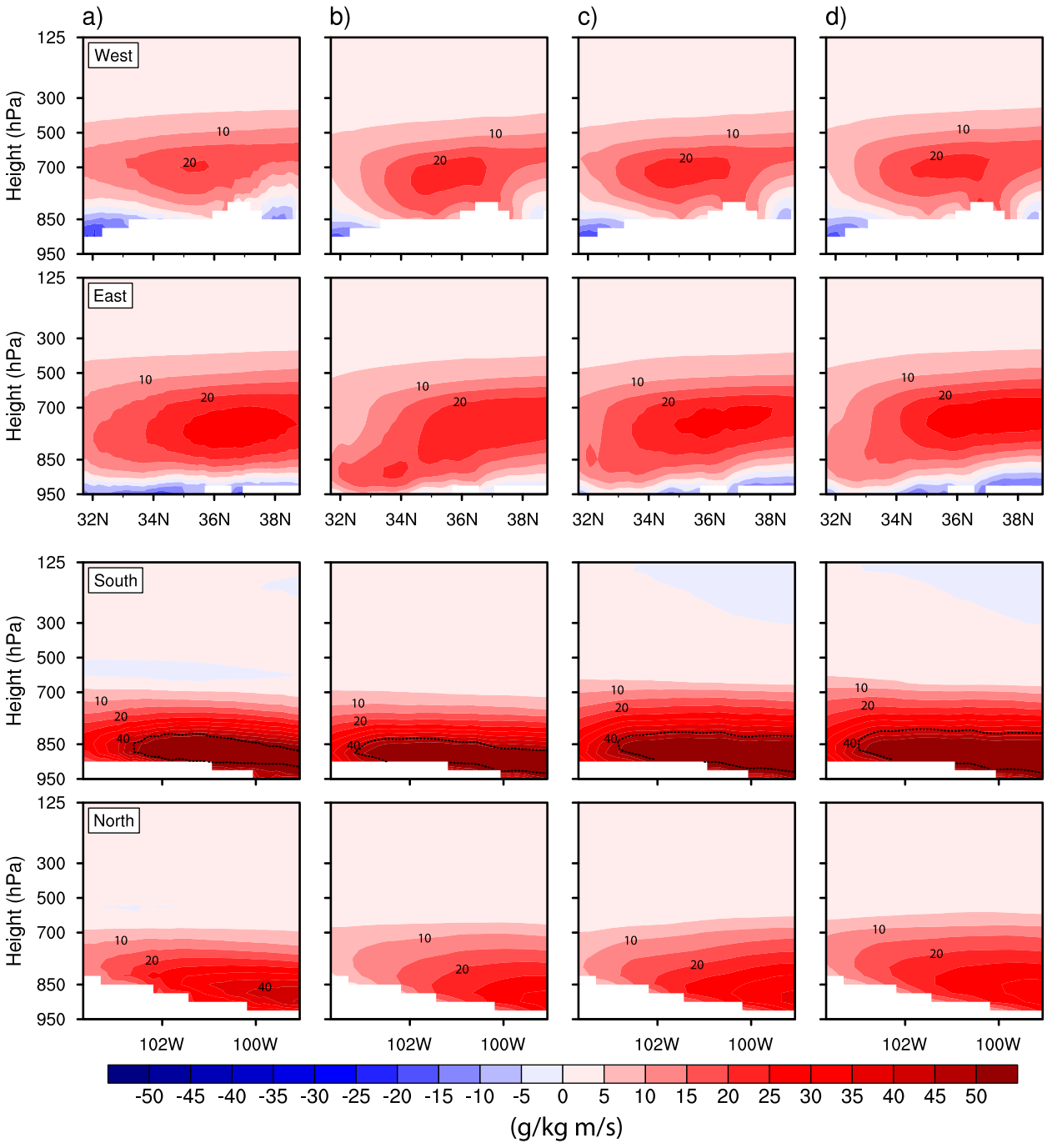

FIG. 6. Growing-season mean moisture flux ($g\,kg^{-1}\,m^{-1}\,s^{-1}$) from (a) NARR, (b) Noah-G3D, (c) Noah-MP-G3D, and (d) Noah-MP-KF at (top)–(bottom) the four lateral boundaries over the SGP averaged over the wet years (1997, 1999, and 2004). Red denotes northward or eastward flow and blue indicates southward or westward flow. The dashed lines in some of the panels outline the region where seasonal averaged daily mean meridional wind speed is $>5\,m\,s^{-1}$.

a stronger sensitivity to the land surface model. All three experiments overestimate the moisture transport into this region from 950 to 700 hPa (source bias in Tables 4 and 5). Noah-G3D has the smallest source bias in both wet and dry years and Noah-MP has 2–3 times the bias of Noah-G3D. The net biases from 950 to 700 hPa (in units of $kg\,kg^{-1}\,m\,s^{-1}$), which represents the moisture flux convergence error in this region, are 2.16 (2.19) in wet (dry) years for Noah-G3D; 3.53 (4.07) in wet (dry) years for Noah-MP-G3D; and 4.40 (5.10) in wet (dry) years for

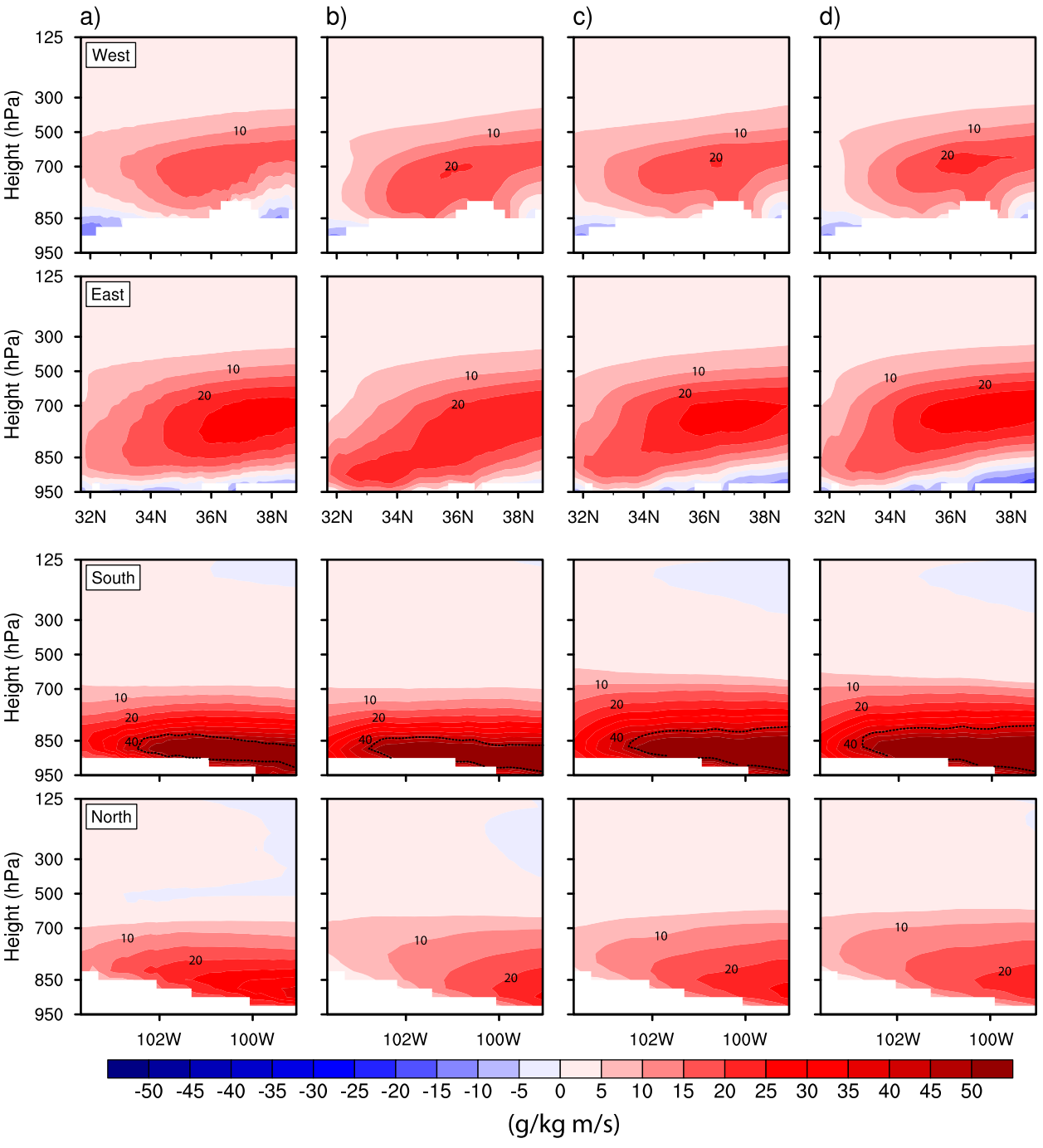

FIG. 7. As in Fig. 6, but for the dry years (1998, 2000, and 2011).

Noah-MP-KF. The Noah-MP-KF has the largest bias both in the moisture source and the net flux in the boundary layer (source bias and net bias in Table 4), with the main wet bias coming from the south. In the midlevel between 850 and 700 hPa (Table 5), the KF scheme better represents the moisture transport from the west boundary both in wet and dry years, where the air parcels and convection cells propagating eastward are highly related to the thermodynamic convective process. This better representation cancels out part of its overestimation in representing the southerly flow and results in better performance for resolving both the moisture source and net flux in this layer than the Noah-MP-G3D.

TABLE 4. Vertically integrated meridional and zonal moisture flux ($kg\,kg^{-1}\,m\,s^{-1}$) and its biases averaged in wet and dry years between 950 and 850 hPa (positive values refer to moisture flows into the SGP and vice versa). (Source bias indicates biases at the southern boundary, and net bias indicates the total bias.)

		NARR	Noah-G3D	Noah-MP-G3D	Noah-MP-KF
Wet	West	−0.58	−0.03	−0.27	−0.24
	East	−0.93	−3.12	−1.58	−0.86
	South	7.24	7.42	7.59	7.83
	North	−2.84	−2.00	−2.32	−2.08
	Zonal	−1.51	−3.15	−1.85	−1.10
	Meridional	4.40	5.42	5.27	5.75
	Source bias	—	0.18	0.35	0.59
	Net bias	—	−0.62	0.53	1.76
Dry	West	−0.30	0.20	−0.05	−0.04
	East	−1.70	−3.73	−1.76	−1.10
	South	6.55	6.84	6.99	7.25
	North	−2.11	−1.39	−1.57	−1.32
	Zonal	−2.00	−3.53	−1.81	−1.14
	Meridional	4.44	5.45	5.42	5.93
	Source bias	—	0.29	0.44	0.70
	Net bias	—	−0.52	1.17	2.35

TABLE 5. As in Table 4, but between 850 and 700 hPa (source bias indicates the integrated bias at the southern and western boundary).

		NARR	Noah-G3D	Noah-MP-G3D	Noah-MP-KF
Wet	West	3.18	4.85	4.46	4.23
	East	−8.56	−7.33	−8.14	−7.81
	South	6.76	5.70	7.79	7.81
	North	−4.76	−3.82	−4.42	−4.97
	Zonal	−5.38	−2.48	−3.68	−3.58
	Meridional	2.00	1.88	3.37	2.84
	Source bias	—	0.61	2.31	2.10
	Net bias	—	2.78	3.07	2.64
Dry	West	3.27	4.81	4.16	3.92
	East	−7.95	−7.32	−7.92	−7.71
	South	6.16	5.56	7.65	7.50
	North	−4.11	−2.97	−3.62	−3.59
	Zonal	−4.68	−2.51	−3.76	−3.79
	Meridional	2.05	2.59	4.03	3.91
	Source bias	—	0.94	2.38	1.99
	Net bias	—	2.71	2.90	2.75

The NARR reanalysis reveals that the major difference between wet and dry years comes from the moisture source from the south being 10% higher in wet years than dry years. Generally speaking, the G3D cumulus parameterization better resolves the Great Plains low-level jet in magnitude than the KF scheme, while Noah better represents the moisture source from 950 to 700 hPa than Noah-MP, which has a very large wet bias. Moisture sources for the SGP between 850 and 700 hPa are bifurcated into two parts—southerly and westerly—both of which, especially the westerly transport, remain a challenge for models to simulate. The main biases in both moisture source and net flux originate from this layer, suggesting difficulties in addressing the dynamics of midlevel moisture convergence and precipitation processes in the regional climate model. A previous study showed that the well-simulated Great Plains low-level jet is not guaranteed for the accurate representation of the rainfall over this area, especially the nocturnal maximum (Jiang et al. 2007; Ghan et al. 1996). When an adequate moisture source is provided, the physics and dynamical processes in the convection schemes are pivotal for the summer rainfall over the SGP yet need to be improved.

c. *Diurnal rainfall and moisture flux variability*

As mentioned earlier, growing-season precipitation over the SGP region is characterized by a pronounced diurnal signal with maximum rainfall usually occurring at night (Dai et al. 1999; Carbone et al. 2002; Carbone and Tuttle 2008; Liang et al. 2004a; Ruane 2010). Thus, it is important to understand how the simulated diurnal cycle of rainfall is affected by the cumulus parameterization and land surface model. The primary factors affecting the diurnal variability of precipitation over the SGP are the diurnal variation of large-scale moisture flux convergence associated with the Great Plains low-level jet (Whiteman et al. 1997) and the thermal instability of the lower atmosphere (local convection and the convective systems propagated eastward from the Rockies). Though the role of the low-level jet as a corridor of enhanced convergence and lifting, moisture transport and frontogenesis has been widely accepted (Tuttle and Davis 2006; Cook et al. 2008), multiple studies have also noted that the eastward propagation of convective systems from the Rockies to the Great Plains plays an essential role in the observed nocturnal rainfall peak in this area and even farther to the east (Maddox 1980; Augustine and Caracena 1994; Carbone et al. 2002; Carbone and Tuttle 2008; Davis et al. 2003; Jiang et al. 2006). For example, by using the NARR reanalysis data, Jiang et al. (2006) found that nearly half of the summer rainfall over the Great Plains is associated with this eastward-propagating system, and with radar observations, the proportion increased to 60% (Carbone and Tuttle 2008). This eastward propagation feature is prominent in the observations of the cases studied here (Fig. 8a). The observed diurnal precipitation evolution in both the wet and dry years illustrate an eastward propagation of the precipitation system at a speed of ~18 $m\,s^{-1}$ between 1900 and 0400 DST (daylight saving time). In wet years, the peak appears mostly to the northeast of the Great Plains low-level jet core (~101°W), which agrees with a previous study showing the associated positive

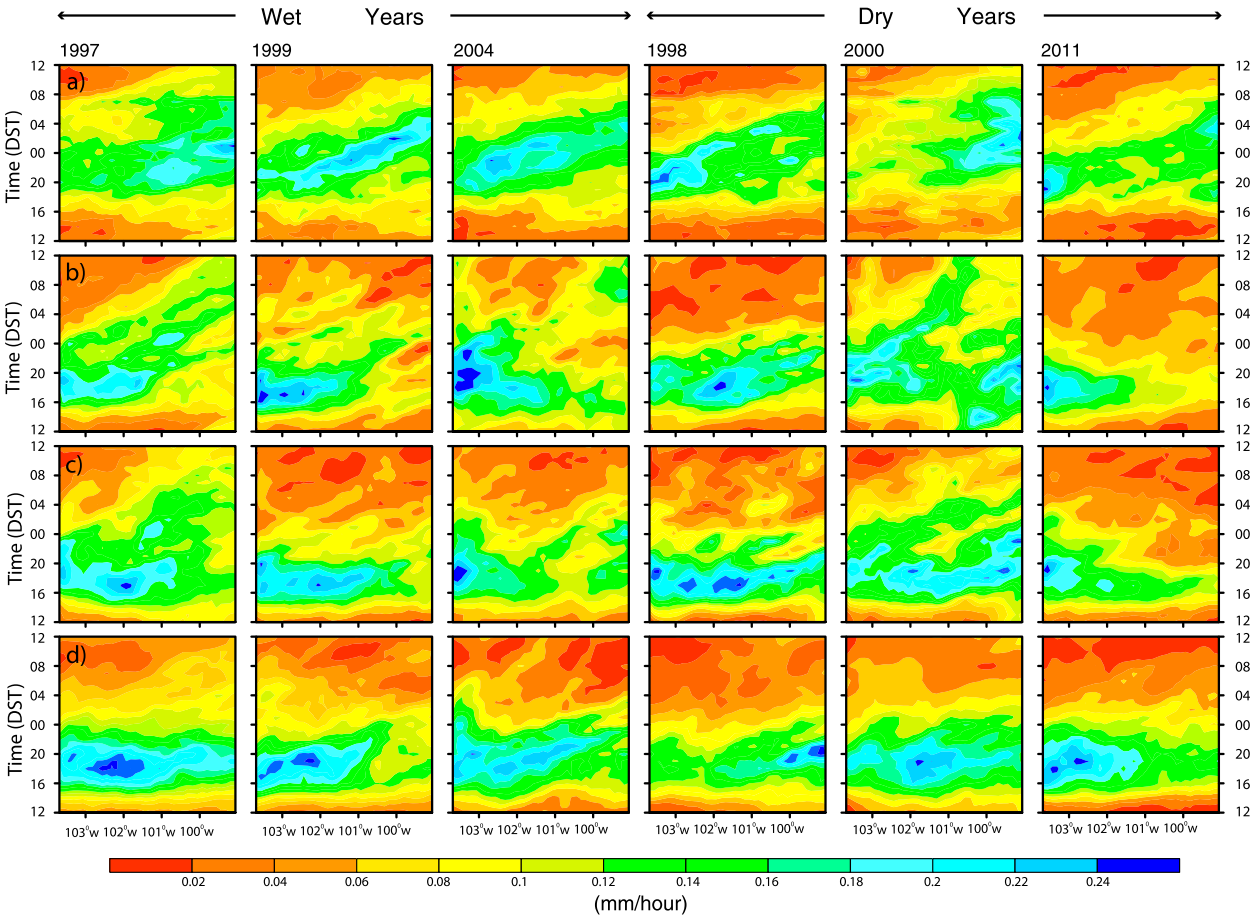

FIG. 8. Hovmöller diagram (DST vs 0.125° longitude bin) of growing-season diurnal precipitation (mm h^{-1}) averaged between 31.688° and 38.813°N for (top)–(bottom) (a) observations, (b) Noah-G3D, (c) Noah-MP-G3D, and (d) Noah-MP-KF and (left)–(right) wet years (1997, 1999, and 2004) and dry years (1998, 2000, and 2011).

precipitation anomalies occurring under the jet-exit region with the strengthening of the low-level jet (Weaver and Nigam 2008). Two out of the three dry years (1998 and 2011) had maximum precipitation near the western boundary around 1900–2000 DST. This difference in the observed pattern between wet and dry years suggests different mechanisms affecting the diurnal rainfall process in the corresponding extreme climate years over the SGP. The models essentially fail to capture this phenomenon (Figs. 8b–d). The simulated precipitation events all tend to appear simultaneously from the west to east too early at around 1600–2000 DST (Figs. 8b–d), with the peak value mostly occurring west of 101.5°W. The differences in spatial distribution are much more obvious between different cumulus parameterizations than between land surface models, with Noah-MP-KF having the largest bias in the rainfall diurnal evolution pattern.

Figure 9 shows comparisons of the simulated growing-season mean diurnal cycles of the spatially averaged rainfall (Fig. 9a) and 2-m air temperature (Fig. 9b) with the NLADS-2 data and the layered atmospheric moisture flux at the western and the southern boundaries of SGP with the NARR data (Figs. 9c–f). The observed precipitation peaks around midnight in wet years and a little earlier in dry years. The simulated precipitation, however, peaks between 1600 and 1800 DST, leading the observed peak by 1–4 h. Noah represents this diurnal variation slightly better than Noah-MP (Fig. 9a). The agreement between the simulated and the observed precipitation amount appears to change depending on the time of day: Noah-G3D agrees reasonably well during daytime hours, but underestimates precipitation at night, while Noah-MP-G3D and Noah-MP-KF substantially overestimate precipitation in the afternoon, but improve at night. Comparing the two cumulus schemes, the peak with the KF scheme is 1–2 h closer in time to the observed peak, but the overestimation is more significant than that with the G3D scheme. The precipitation anomalies are usually related to the temperature anomalies, but all three experiments capture the diurnal variation of 2-m

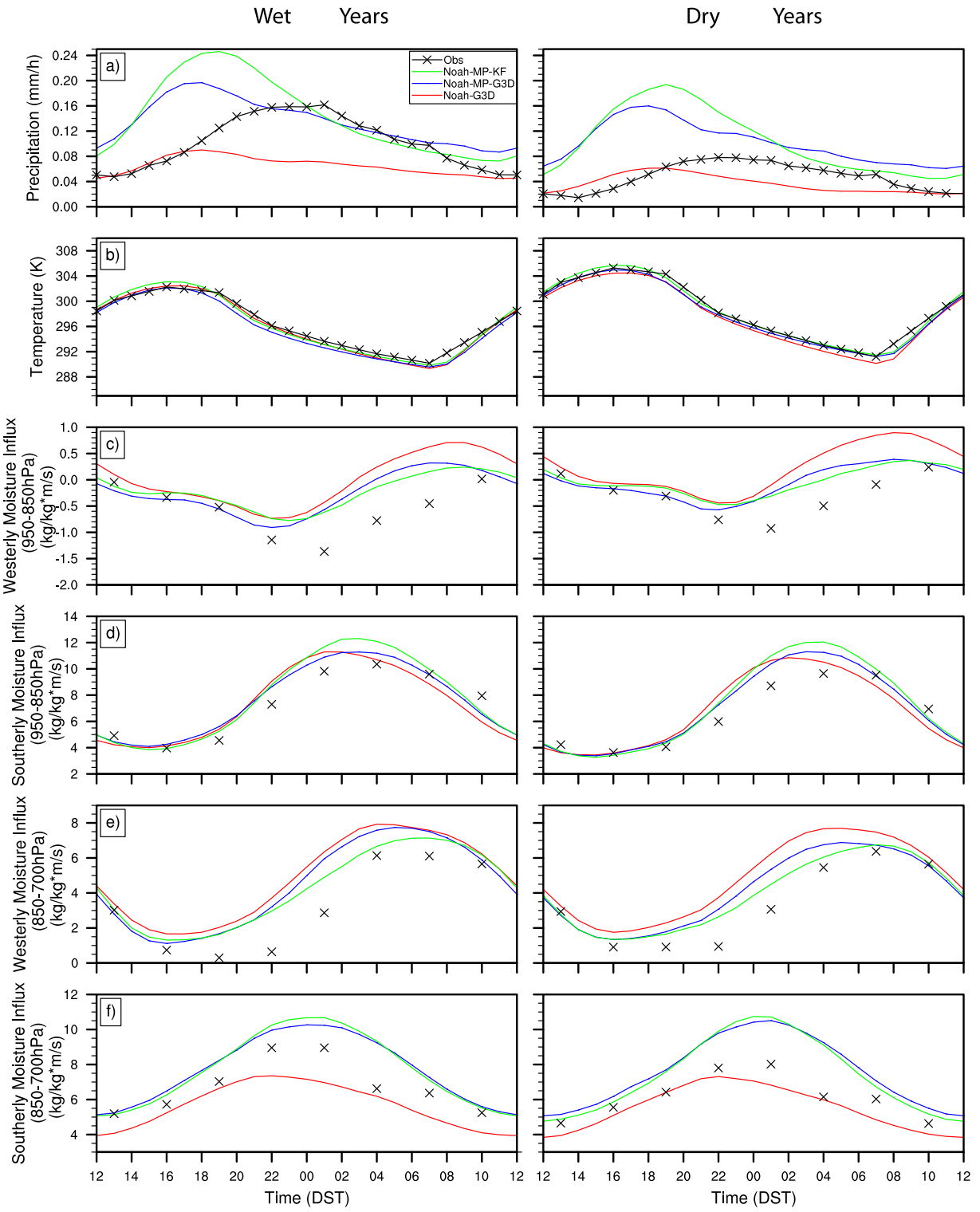

FIG. 9. (left) Wet-year and (right) dry-year averaged diurnal variations of (top)–(bottom) (a) precipitation (mm h^{-1}) and (b) 2-m air temperature (K); vertically integrated moisture flux (kg kg^{-1} m s^{-1}) between 950 and 850 hPa at (c) the western and (d) the southern lateral boundaries; vertically integrated moisture flux (kg kg^{-1} m s^{-1}) between 850 and 700 hPa at (e) the western and (f) the southern lateral boundaries over the SGP. Black crosses in the moisture flux denote NARR reanalysis and the black line with crosses denotes NLDAS-2 forcing datasets. A positive value in the moisture flux indicates moisture imported into the region and vice versa.

air temperature reasonably well both in phase and magnitude (Fig. 9b).

The westerly and southerly moisture fluxes (Figs. 9c–f) refer to the vertically integrated moisture flux at the western and southern boundary in the corresponding layer. All simulations capture these flux variations reasonably well. The westerly moisture flow at the western boundary represents the eastward-propagating convection systems into the western boundary of the SGP region, while the southerly moisture flow at the southern boundary represents the moisture transport mainly from the Gulf of Mexico northward into the SGP by the low-level jet. The patterns and magnitudes of the southerly moisture flux between 950 and 850 hPa (Fig. 9d) are well simulated, and the differences between wet and dry years are small both in the NARR reanalysis and model outputs. This indicates that the moisture carried by the low-level jet into the SGP below 850 hPa is not a limiting factor to the precipitation differences between the wet and dry years.

The phase of the low-level jet variation (Fig. 9d) coincides well with that of the westerly flow aloft between 850 and 700 hPa (Fig. 9e). This overlay structure produces vertical wind shear that favors persistence of deep convection and helps organize small convective systems into larger convective complexes. The veering wind profile is also indicative of warm advection that is typically associated with mesoscale upward motion, which is important to maintain many nocturnal mesoscale convective systems. In the cases studied here, this mechanism is also strengthened by the climax of meridional midlevel (850–700 hPa) moisture flux around midnight (Fig. 9f). All experiments capture these moisture flux variations quite well, but all fail to represent the nocturnal maximum precipitation, suggesting possible deficiencies in the cumulus parameterizations in depicting deep convection. The outflow at the lower western boundary caused by the mountain–plain circulation during daytime is well captured in all experiments (1000–1900 DST, Fig. 9c). But the nighttime divergence is considerably lower than that of NARR (2200–0700 DST, Fig. 9c). This is partly due to the simulations missing the nocturnal maximum precipitation, which induces subsidence over the SGP and thus outflow in the western lower boundary.

It is noteworthy that the largest discrepancies between the moisture fluxes simulated by the three experiments exist in the southern boundary, between 850 and 700 hPa (Fig. 9f), with the Noah-MP significantly enhancing the moisture flux especially around midnight. The Noah-G3D moisture flux is about 30% (daytime) to 50% (nighttime) lower compared to the moisture flux in the Noah-MP-based simulations, generating more accurate variations in dry years, with comparable biases in wet years (Fig. 9f). Aside from the overestimation in this incoming moisture flux into the SGP, Noah-MP also considerably overestimates the net meridional moisture convergence over this region (Table 5). Zhang and Klein (2010) investigated the mechanisms affecting the transition from shallow to deep convection over the SGP by using the observed diurnal cycle data, suggesting that the moisture content above the boundary layer is critical for the early onset of the afternoon precipitation events as well as its duration. Studies also showed direct connection between the increased midlevel moisture convergence and the enhanced rainfall (Cook et al. 2008). The overestimation of the midlevel meridional moisture convergence by Noah-MP-based simulations directly contributes to the overestimated rainfall amount and its earlier peaking in late afternoon (Fig. 9a).

In general, the impact of the two land surface models on the moisture flux is significantly higher than that of the cumulus parameterizations, and thus has a larger effect on the diurnal rainfall variation (especially the intensity). By investigating the normalized covariance between the atmospheric water budget components and rainfall on diurnal scales over the Great Plains, Ruane (2010) concluded that subsidence induced by large-scale mountain–plain circulation helps accumulate the inhibitive convective energy during the daytime, which is then released by the eastward-propagating convective system at night and triggers nocturnal precipitation. The low-level jet then acts as a moisture corridor contributing to the strengthening of convection, generating spectacular storms at night. Because of the deficiencies in the cumulus parameterizations, appropriate representations of this diurnal feature still remain problematic and challenging for most regional climate models.

d. Surface energy flux and 2-m air temperature

In an attempt to explain the large systematic differences in the simulated precipitation amount and atmospheric moisture flux between Noah and Noah-MP, the simulated monthly averaged surface latent heat fluxes (the energy form of ET; Fig. 10) are compared with the MOD16 datasets (Mu et al. 2011). The MOD16 monthly surface latent heat flux dataset covers 2000–13, overlapping three of our studied years (2000, 2004, and 2011). Previous studies have shown an important connection between local precipitation and the upstream ET (Georgescu et al. 2003; Laird et al. 2010). Here, the spatially averaged latent heat flux from both the SGP region and the upstream area (Fig. 2, green rectangle, defined by the 850-hPa wind fields, not shown) for the three overlapping years are examined. As shown in Fig. 10, the trend of the monthly variation in MOD16 is captured by both land surface models, though Noah-MP provides significant overestimates in

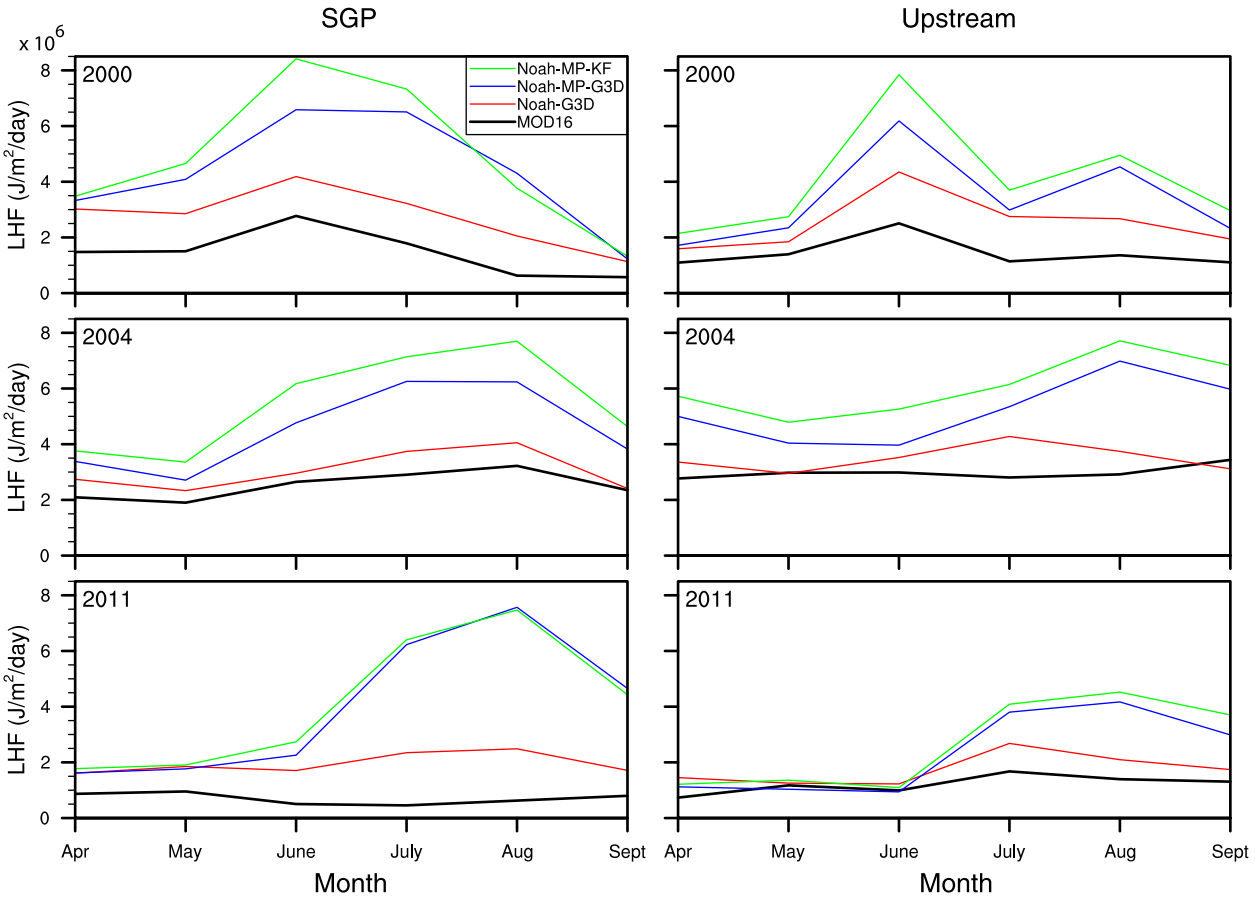

FIG. 10. Monthly mean surface latent heat flux ($J\,m^{-2}\,day^{-1}$) over (left) the SGP and (right) the upstream area (Fig. 2) from the simulations and the MOD16 datasets: (top)–(bottom) 2000, 2004, and 2011.

both the SGP and the upstream area for all three years. The overestimation of ET by Noah-MP was also found in Cai et al. (2014), based on an offline study of the hydrological cycle in the Mississippi River basin over four different vegetation types (grassland, cropland, forest, and shrubland). As implied by the authors (Cai et al. 2014), a possible reason for this overestimate of ET by Noah-MP is the overpredicted leaf area index (LAI) by the dynamic leaf model (Dickinson et al. 1998; Yang and Niu 2003; Niu et al. 2011) that was incorporated into Noah-MP. This, however, does not appear to be the case in our study because the predicted LAI in Noah-MP is smaller than the prescribed LAI in Noah (not shown) although the vegetation cover in SGP and the upstream areas is dominated by grassland. Instead, significantly higher top layer soil moisture is produced by Noah-MP (Fig. 11) during summer (May–August), contributing directly to the overestimated ET. The ET estimates are also too large in the original Noah land surface model, especially in wet years, though the magnitudes of the differences are much smaller. Overestimation of ET on grassland with Noah in summer months was also noted in Jaksa et al. (2013).

The simulated 2-m air temperatures (Fig. 12) are reasonably accurate during the spring, with more discrepancies among three experiments in the summer when the simulated Bowen ratio (ratio of sensible heat flux to latent heat flux, not shown) also differs the most among the experiments. Smaller simulated sensible heat fluxes (not shown) are found in Noah-MP-based simulations, which correspond to the underestimation of the air temperature by as much as 5 K, while Noah-G3D yields temperature fluctuations that are closer to the observed fluctuations, with cold biases mostly within 3 K.

4. Summary and discussion

The current study examined the sensitivity of WRF simulations of growing-season hydrologic cycle over the SGP to the choices of cumulus parameterization schemes and land surface models in the unusually wet and dry years. Specifically, two cumulus parameterizations—G3D and KF—and two land surface models—Noah and Noah-MP—are tested.

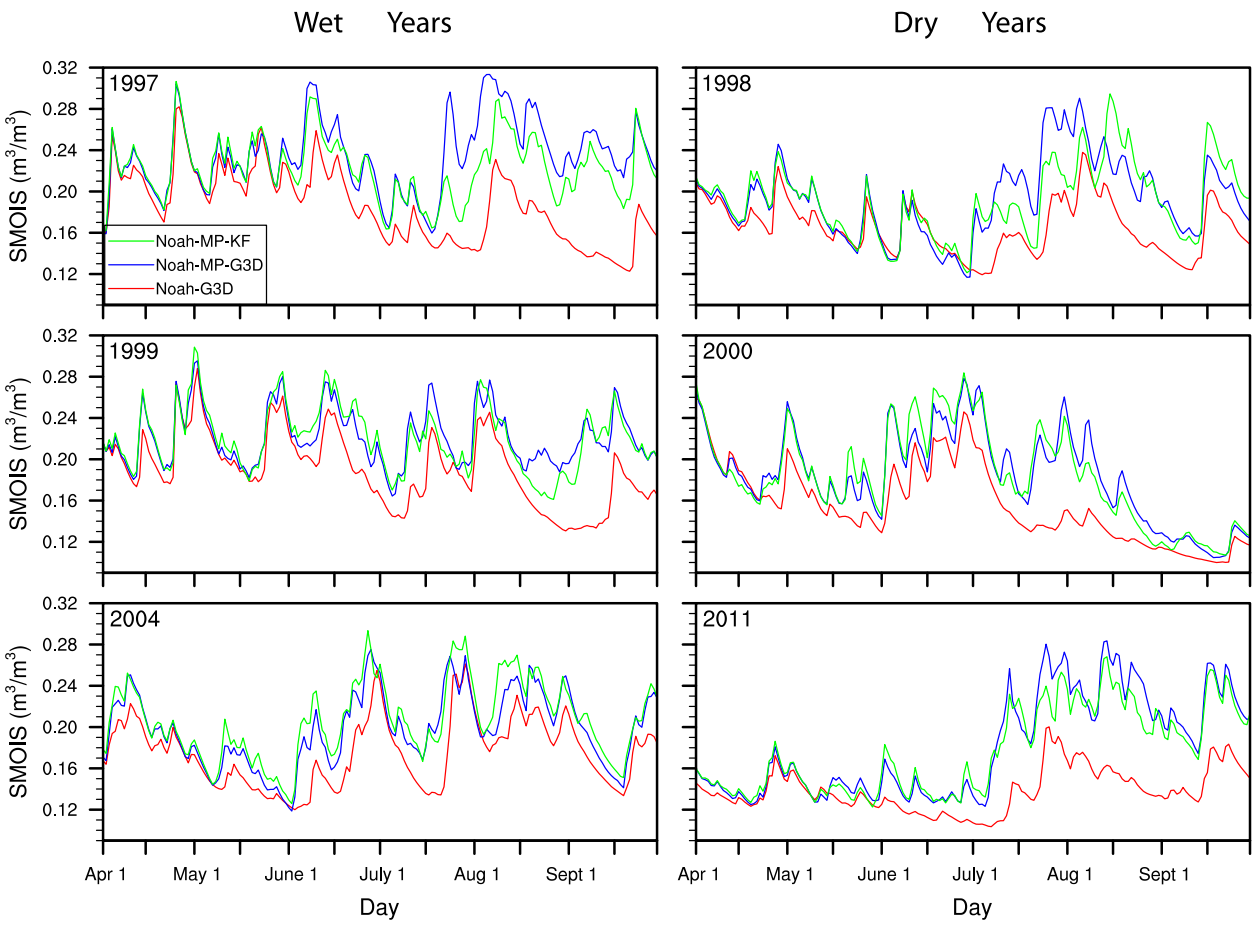

FIG. 11. Simulated daily mean top layer soil moisture ($m^3\ m^{-3}$) over the SGP for (top)–(bottom) (left) wet years (1997, 1999, and 2004) and (right) dry years (1998, 2000, and 2011).

The main difference between the wet and dry years in the atmospheric moisture source lies in the intensity of the Great Plains low-level jet. In wet years, a stronger low-level jet favors the intensification of rainfall to the northeast of the jet-exit region; while in dry years the core of precipitation shifts westward to the western boundary of the SGP and occurs earlier, with thermal instability contributing more to the precipitation process. Our results show significant modifications by the Noah-MP over Noah in surface energy fluxes and the atmospheric water budget, with the former significantly increasing surface ET and enhancing the moisture flux convergence in this region, resulting in considerable rainfall overestimation. In general, the Noah-G3D exhibits the smallest total error in the simulated daily precipitation amount in both wet and dry years; it best captures both the spatial distribution of the mean daily precipitation and diurnal variation of rainfall in dry years, but has errors that are comparable to those with Noah-MP in wet years.

Compared with the cumulus parameterization scheme, the land surface model exerts larger influence on the simulated diurnal rainfall variability as well. The eastward propagation of the convective systems from the Rockies, an important factor for precipitation over SGP, has been difficult for most numerical weather models to simulate (Davis et al. 2003) and is not well captured by either of the two cumulus parameterizations applied here. Appropriate representation of the rainfall diurnal features over the SGP by numerical models requires the following: 1) accurately resolving the elevated topographic heating source and initialization of the convection along the eastern slope of the Rockies, 2) accurately depicting the eastward propagation of convective systems under favorable large-scale synoptic flow and vertical wind shear conditions, 3) adequately describing the dynamics of the Great Plains low-level jet both in phase and amplitude, and 4) incorporating a cumulus parameterization that includes the interactions of the physical processes stated above. Both cumulus parameterizations applied in this study remain problematic in representing most of these features, suggesting that further attention and improvements are necessary.

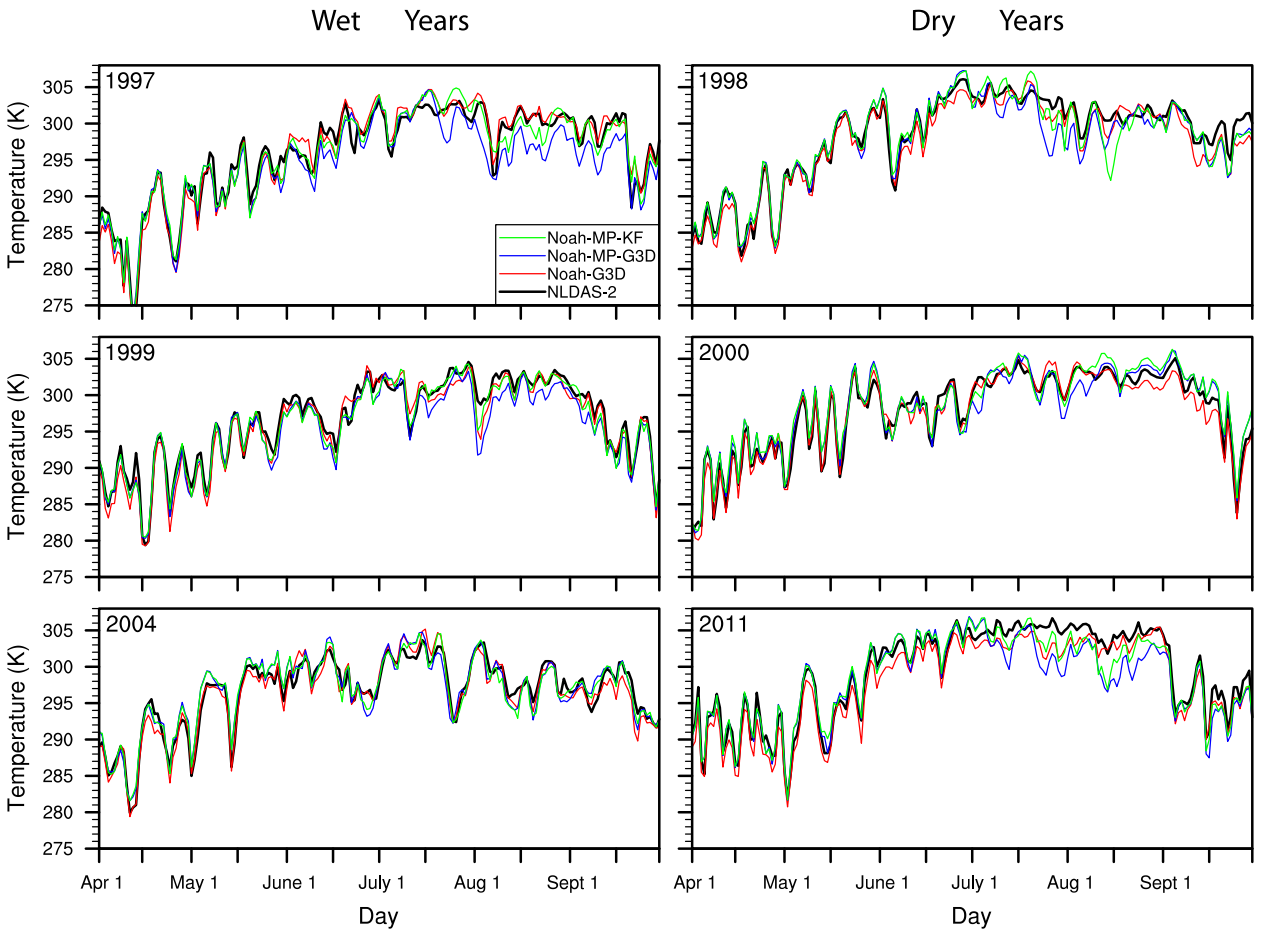

FIG. 12. Daily mean 2-m air temperature (K) over the SGP from the simulations and the NLDAS-2 forcing datasets: (top)–(bottom) (left) wet years (1997, 1999, and 2004) and (right) dry years (1998, 2000, and 2011).

Major improvements from Noah to Noah-MP include the canopy process, groundwater interaction, and the snow process. For the simulated growing-season extreme climates over the SGP, the canopy process and groundwater interaction are expected to account for most of the differences generated between these two land surface models. The dynamic leaf model in the canopy module of Noah-MP, however, underestimates the LAI significantly relative to the prescribed LAI from the National Oceanic and Atmospheric Administration/Advanced Very High Resolution Radiometer (NOAA/AVHRR) used in Noah, which can significantly reduce the canopy portion of ET and increase the bare soil evaporation. Also as a landscape featuring an underlying aquifer system, the inclusion of groundwater processes is critical to produce a reasonable representation of the coupled water cycle in the subsurface. But because of uncertainties in the deep soil textures and the related hydraulic parameters, the initial condition errors, and coarse model resolution, the water table depth remains difficult to simulate in the current Noah-MP groundwater module. Cai et al. (2014) concluded that the differences between the simulated water table depth (2–14 m) by Noah-MP in the Mississippi River basin and the observed one (around 0–80 m) is mainly caused by the coarse spatial resolution, which is 0.125° in their study.

The significant overestimate of surface ET with Noah-MP may be associated with three main factors. First, less LAI is predicted by the dynamic leaf model, which reduces canopy interception and enhances soil moisture. Second, it is difficult to calibrate three soil parameters (surface dryness factor, saturated hydraulic conductivity, and saturated soil moisture) that are considered to be highly sensitive for Noah-MP to simulate the land surface hydrologic cycle. All three parameters remain highly uncertain for deep soil layers in different regions, and are difficult to calibrate, especially in the arid and semiarid regions (Cai et al. 2014). Third, there are possible interactive problems with the boundary layer scheme. The land surface model and the planetary boundary layer

schemes strongly interact with each other in calculating the lower-atmosphere temperature and moisture tendencies (Zhong and Doran 1995, 1997; Steeneveld et al. 2006; Santanello et al. 2007). The development of the low-level jet, a key factor for the moisture transport in this region, relies heavily on the boundary layer physics (Qian et al. 2013). There are multiple choices of boundary layer schemes, and for this study the Mellor–Yamada–Janjić (MYJ) scheme (Mellor and Yamada 1982; Janjić 1990, 1994, 2001) is used. It is possible that the results may change when a different boundary layer scheme is coupled with Noah and Noah-MP, yet testing all possible coupling is beyond the scope of this study. Model errors can also be caused by the impacts of irrigation over this area, whose effect on the regional climate should not be ignored (DeAngelis et al. 2010; Harding and Snyder 2012a,b; Leng et al. 2013; Qian et al. 2013).

Acknowledgments. This research was supported partially by the U.S. National Science Foundation (CR-Water Sustainability and Climate 1039180), the U.S. Forest Service Northern Research Station (Research Joint Venture Agreement 11-JV-11242306-065), and the Chinese Academy of Sciences (Strategic Priority Research Program Grant XDA05110101). The views expressed are those of the authors and do not necessarily reflect those of the sponsoring agencies. We thank Anthony D. Kendall, Xindi Bian, and two anonymous reviewers for their constructive comments. We also acknowledge the Institute for Cyber-Enabled Research of Michigan State University for the computational resources, especially for the assistance from Dr. Benjamin Ong, and the visualization support from the NCAR Command Language (2012).

REFERENCES

Augustine, J. A., and F. Caracena, 1994: Lower-tropospheric precursors to nocturnal MCS development over the central United States. *Wea. Forecasting,* **9,** 116–135, doi:10.1175/1520-0434(1994)009<0116:LTPTNM>2.0.CO;2.

Barnston, A. G., and P. T. Schickedanz, 1984: The effect of irrigation on warm season precipitation in the Southern Great Plains. *J. Climate Appl. Meteor.,* **23,** 865–888, doi:10.1175/1520-0450(1984)023<0865:TEOIOW>2.0.CO;2.

Basso, B., A. D. Kendall, and D. W. Hyndman, 2013: The future of agriculture over the Ogallala Aquifer: Solutions to grow crops more efficiently with limited water. *Earth's Future,* **1,** 39–41, doi:10.1002/2013EF000107.

Betts, A. K., and M. J. Miller, 1993: The Betts-Miller scheme. *The Representation of Cumulus Convection in Numerical Models of the Atmosphere, Meteor. Monogr.,* No. 46, Amer. Meteor. Soc., 107–121.

Beven, K. J., and M. J. Kirkby, 1979: A physically based variable contributing area model of basin hydrology. *Hydrol. Sci. Bull.,* **24,** 43–69, doi:10.1080/02626667909491834.

Cai, X., Z.-L. Yang, C. H. David, G.-Y. Niu, and M. Rodell, 2014: Hydrological evaluation of the Noah-MP land surface model for the Mississippi River Basin. *J. Geophys. Res. Atmos.,* **119,** 23–38, doi:10.1002/2013JD020792.

Carbone, R. E., and J. D. Tuttle, 2008: Rainfall occurrence in the U.S. warm season: The diurnal cycle. *J. Climate,* **21,** 4132–4146, doi:10.1175/2008JCLI2275.1.

——, ——, D. A. Ahijevych, and S. B. Trier, 2002: Inferences of predictability associated with warm season precipitation episodes. *J. Atmos. Sci.,* **59,** 2033–2056, doi:10.1175/1520-0469(2002)059<2033:IOPAWW>2.0.CO;2.

Chen, F., and Coauthors, 1996: Modeling of land surface evaporation by four schemes and comparison with FIFE observations. *J. Geophys. Res.,* **101,** 7251–7268, doi:10.1029/95JD02165.

Chen, J., and P. Kumar, 2001: Topographic influence on the seasonal and interannual variation of water and energy balance of basins in North America. *J. Climate,* **14,** 1989–2014, doi:10.1175/1520-0442(2001)014<1989:TIOTSA>2.0.CO;2.

Choi, H. I., and X.-Z. Liang, 2010: Improved terrestrial hydrologic representation in mesoscale land surface models. *J. Hydrometeor.,* **11,** 797–809, doi:10.1175/2010JHM1221.1.

Cook, K. H., E. K. Vizy, Z. S. Launer, and C. M. Patricola, 2008: Springtime intensification of the Great Plains low-level jet and midwest precipitation in GCM simulations of the twenty-first century. *J. Climate,* **21,** 6321–6340, doi:10.1175/2008JCLI2355.1.

Cosgrove, B. A., and Coauthors, 2003: Real-time and retrospective forcing in the North American Land Data Assimilation System (NLDAS) project. *J. Geophys. Res.,* **108,** 8842, doi:10.1029/2002JD003118.

Dai, A., F. Giorgi, and K. E. Trenberth, 1999: Observed and model-simulated diurnal cycles of precipitation over the contiguous United States. *J. Geophys. Res.,* **104,** 6377–6402, doi:10.1029/98JD02720.

Davis, C. A., K. W. Manning, R. E. Carbone, S. B. Trier, and J. D. Tuttle, 2003: Coherence of warm-season continental rainfall in numerical weather prediction models. *Mon. Wea. Rev.,* **131,** 2667–2679, doi:10.1175/1520-0493(2003)131<2667:COWCRI>2.0.CO;2.

DeAngelis, A., F. Dominguez, Y. Fan, A. Robock, M. D. Kustu, and D. Robinson, 2010: Evidence of enhanced precipitation due to irrigation over the Great Plains of the United States. *J. Geophys. Res.,* **115,** D15115, doi:10.1029/2010JD013892.

——, A. J. Broccoli, and S. G. Decker, 2013: A comparison of CMIP3 simulations of precipitation over North America with observations: Daily statistics and circulation features accompanying extreme events. *J. Climate,* **26,** 3209–3230, doi:10.1175/JCLI-D-12-00374.1.

De Haan, L. L., M. Kanamitsu, C.-H. Lu, and J. O. Roads, 2007: A comparison of the Noah and OSU land surface models in the ECPC seasonal forecast model. *J. Hydrometeor.,* **8,** 1031–1048, doi:10.1175/JHM629.1.

Dickinson, R. E., R. M. Errico, F. Giorgi, and G. T. Bates, 1989: A regional climate model for the western United States. *Climatic Change,* **15,** 383–422, doi:10.1007/BF00240465.

——, M. Shaikh, R. Bryant, and L. Graumlich, 1998: Interactive canopies for a climate model. *J. Climate,* **11,** 2823–2836, doi:10.1175/1520-0442(1998)011<2823:ICFACM>2.0.CO;2.

Dudhia, J., 1989: Numerical study of convection observed during the winter monsoon experiment using a mesoscale two-dimensional model. *J. Atmos. Sci.,* **46,** 3077–3107, doi:10.1175/1520-0469(1989)046<3077:NSOCOD>2.0.CO;2.

Ek, M. B., K. E. Mitchell, Y. Lin, E. Rogers, P. Grunmann, V. Koren, G. Gayno, and J. D. Tarpley, 2003: Implementation of Noah land surface model advances in the National Centers

for Environmental Prediction operational mesoscale Eta model. *J. Geophys. Res.,* **108,** 8851, doi:10.1029/2002JD003296.

Emanuel, R. E., A. G. Hazen, B. L. McGlynn, and K. G. Jencso, 2014: Vegetation and topographic influences on the connectivity of shallow groundwater between hillslopes and streams. *Ecohydrology,* **7,** 887–895, doi:10.1002/eco.1409.

Emori, S., A. Hasegawa, T. Suzuki, and K. Dairaku, 2005: Validation, parameterization dependence, and future projection of daily precipitation simulated with a high-resolution atmospheric GCM. *Geophys. Res. Lett.,* **32,** L06708, doi:10.1029/2004GL022306.

Fan, Y., G. Miguez-Macho, C. P. Weaver, R. Walko, and A. Robock, 2007: Incorporating water table dynamics in climate modeling: 1. Water table observations and equilibrium water table simulations. *J. Geophys. Res.,* **112,** D10125, doi:10.1029/2006JD008111.

Garrett, C., and P. Müller, 2008: Supplement to extreme events. *Bull. Amer. Meteor. Soc.,* **89,** ES45–ES56, doi:10.1175/2008BAMS2566.2.

Georgescu, M., C. P. Weaver, R. Avissar, R. L. Walko, and G. Miguez-Macho, 2003: Sensitivity of model-simulated summertime precipitation over the Mississippi River Basin to the spatial distribution of initial soil moisture. *J. Geophys. Res.,* **108,** 8855, doi:10.1029/2002JD003107.

Ghan, S. J., X. Bian, and L. Corsetti, 1996: Simulation of the Great Plains low-level jet and associated clouds by general circulation models. *Mon. Wea. Rev.,* **124,** 1388–1408, doi:10.1175/1520-0493(1996)124<1388:SOTGPL>2.0.CO;2.

Grell, G. A., 1993: Prognostic evaluation of assumptions used by cumulus parameterizations. *Mon. Wea. Rev.,* **121,** 764–787, doi:10.1175/1520-0493(1993)121<0764:PEOAUB>2.0.CO;2.

——, and D. Devenyi, 2002: A generalized approach to parameterizing convection combining ensemble and data assimilation techniques. *Geophys. Res. Lett.,* **29,** doi:10.1029/2002GL015311.

Harding, K. J., and P. K. Snyder, 2012a: Modeling the atmospheric response to irrigation in the Great Plains. Part I: General impacts on precipitation and the energy budget. *J. Hydrometeor.,* **13,** 1667–1686, doi:10.1175/JHM-D-11-098.1.

——, and ——, 2012b: Modeling the atmospheric response to irrigation in the Great Plains. Part II: The precipitation of irrigated water and changes in precipitation recycling. *J. Hydrometeor.,* **13,** 1687–1703, doi:10.1175/JHM-D-11-099.1.

Higgins, R. W., Y. Yao, E. S. Yarosh, J. E. Janowiak, and K. C. Mo, 1997: Influence of the Great Plains low-level jet on summertime precipitation and moisture transport over the central United States. *J. Climate,* **10,** 481–507, doi:10.1175/1520-0442(1997)010<0481:IOTGPL>2.0.CO;2.

Hoch, J., and P. Markowski, 2005: A climatology of springtime dryline position in the U.S. Great Plains region. *J. Climate,* **18,** 2132–2137, doi:10.1175/JCLI3392.1.

Hogue, T. S., L. Bastidas, H. Gupta, S. Sorooshian, K. Mitchell, and W. Emmerich, 2005: Evaluation and transferability of the Noah land surface model in semiarid environments. *J. Hydrometeor.,* **6,** 68–84, doi:10.1175/JHM-402.1.

Hong, S.-Y., and J.-O. J. Lim, 2006: The WRF single-moment 6-class microphysics scheme (WSM6). *J. Korean Meteor. Soc.,* **42** (2), 129–151.

Iorio, J. P., P. B. Duffy, B. Govindasamy, S. L. Thompson, M. Khairoutdinov, and D. Randall, 2004: Effects of model resolution and subgrid-scale physics on the simulation of precipitation in the continental United States. *Climate Dyn.,* **23,** 243–258, doi:10.1007/s00382-004-0440-y.

Jaksa, W. T., V. Sridhar, J. L. Huntington, and M. Khanal, 2013: Evaluation of the complementary relationship using Noah land surface model and North American Regional Reanalysis (NARR) data to estimate evapotranspiration in semiarid ecosystems. *J. Hydrometeor.,* **14,** 345–359, doi:10.1175/JHM-D-11-067.1.

Janjić, Z. I., 1990: The step-mountain coordinate: Physical package. *Mon. Wea. Rev.,* **118,** 1429–1443, doi:10.1175/1520-0493(1990)118<1429:TSMCPP>2.0.CO;2.

——, 1994: The step-mountain Eta coordinate model: Further developments of the convection, viscous layer, and turbulence closure schemes. *Mon. Wea. Rev.,* **122,** 927–945, doi:10.1175/1520-0493(1994)122<0927:TSMECM>2.0.CO;2.

——, 2001: Nonsingular implementation of the Mellor-Yamada level 2.5 scheme in the NCEP Meso model. NOAA/NWS/NCEP Office Note 437, 61 pp.

Jiang, X., N.-C. Lau, and S. A. Klein, 2006: Role of eastward propagating convection systems in the diurnal cycle and seasonal mean of summertime rainfall over the U.S. Great Plains. *Geophys. Res. Lett.,* **33,** L19809, doi:10.1029/2006GL027022.

——, ——, I. M. Held, and J. J. Ploshay, 2007: Mechanisms of the Great Plains low-level jet as simulated in an AGCM. *J. Atmos. Sci.,* **64,** 532–547, doi:10.1175/JAS3847.1.

Kain, J. S., 2004: The Kain–Fritsch convective parameterization: An update. *J. Appl. Meteor.,* **43,** 170–181, doi:10.1175/1520-0450(2004)043<0170:TKCPAU>2.0.CO;2.

——, and J. M. Fritsch, 1993: Convective parameterization in mesoscale models: The Kain-Fritsch scheme. *The Representation of Cumulus Convection in Numerical Models, Meteor. Monogr.,* Vol. 46, Amer. Meteor. Soc., 165–170.

Kanemasu, E. T., J. L. Steiner, A. W. Biere, F. D. Worman, and J. F. Stone, 1983: Irrigation in the Great Plains. *Agric. Water Manage.,* **7,** 157–178, doi:10.1016/0378-3774(83)90080-X.

Kharin, V. V., F. W. Zwiers, X. Zhang, and G. C. Hegerl, 2007: Changes in temperature and precipitation extremes in the IPCC ensemble of global coupled model simulations. *J. Climate,* **20,** 1419–1444, doi:10.1175/JCLI4066.1.

Kimoto, M., N. Yasutomi, C. Yokoyama, and S. Emori, 2005: Projected changes in precipitation characteristics around Japan under the global warming. *SOLA,* **1,** 85–88, doi:10.2151/sola.2005-023.

Kollet, S. J., and R. M. Maxwell, 2008: Capturing the influence of groundwater dynamics on land surface processes using an integrated, distributed watershed model. *Water Resour. Res.,* **44,** W02402, doi:10.1029/2007WR006004.

Koster, R. D., and Coauthors, 2004: Regions of strong coupling between soil moisture and precipitation. *Science,* **305,** 1138–1140, doi:10.1126/science.1100217.

Kuo, H. L., 1974: Further studies of the parameterization of the influence of cumulus convection on large-scale flow. *J. Atmos. Sci.,* **31,** 1232–1240, doi:10.1175/1520-0469(1974)031<1232:FSOTPO>2.0.CO;2.

Laird, N., R. Sobash, and N. Hodas, 2010: Climatological conditions of lake-effect precipitation events associated with the New York State Finger Lakes. *J. Appl. Meteor. Climatol.,* **49,** 1052–1062, doi:10.1175/2010JAMC2312.1.

Lee, M.-I., I. Choi, W.-K. Tao, S. D. Schubert, and I.-S. Kang, 2010: Mechanisms of diurnal precipitation over the U.S. Great Plains: A cloud resolving model perspective. *Climate Dyn.,* **34,** 419–437, doi:10.1007/s00382-009-0531-x.

Leng, G., M. Huang, Q. Tang, W. J. Sacks, H. Lei, and L. R. Leung, 2013: Modeling the effects of irrigation on land surface fluxes and states over the conterminous United States: Sensitivity to input data and model parameters. *J. Geophys. Res. Atmos.,* **118,** 9789–9803, doi:10.1002/jgrd.50792.

——, ——, ——, H. Gao, and L. R. Leung, 2014: Modeling the effects of groundwater-fed irrigation on terrestrial hydrology over the conterminous United States. *J. Hydrometeor.,* **15,** 957–972, doi:10.1175/JHM-D-13-049.1.

Leung, L. R., L. O. Mearns, F. Giorgi, and R. L. Wilby, 2003: Regional climate research needs and opportunities. *Bull. Amer. Meteor. Soc.,* **84,** 89–95, doi:10.1175/BAMS-84-1-89.

Liang, X.-Z., L. Li, A. Dai, and K. E. Kunkel, 2004a: Regional climate model simulation of summer precipitation diurnal cycle over the United States. *Geophys. Res. Lett.,* **31,** L24208, doi:10.1029/2004GL021054.

——, ——, K. E. Kunkel, M. Ting, and J. X. L. Wang, 2004b: Regional climate model simulation of U.S. precipitation during 1982–2002. Part I: Annual cycle. *J. Climate,* **17,** 3510–3528, doi:10.1175/1520-0442(2004)017<3510:RCMSOU>2.0.CO;2.

——, M. Xu, K. E. Kunkel, G. A. Grell, and J. S. Kain, 2007: Regional climate model simulation of U.S.–Mexico summer precipitation using the optimal ensemble of two cumulus parameterizations. *J. Climate,* **20,** 5201–5207, doi:10.1175/JCLI4306.1.

——, and Coauthors, 2012: Regional climate–weather research and forecasting model. *Bull. Amer. Meteor. Soc.,* **93,** 1363–1387, doi:10.1175/BAMS-D-11-00180.1.

Luo, L., and Coauthors, 2003: Validation of the North American Land Data Assimilation System (NLDAS) retrospective forcing over the southern Great Plains. *J. Geophys. Res.,* **108,** 8843, doi:10.1029/2002JD003246.

Maddox, R. A., 1980: Mesoscale convective complexes. *Bull. Amer. Meteor. Soc.,* **61,** 1374–1387, doi:10.1175/1520-0477(1980)061<1374:MCC>2.0.CO;2.

Mahmood, R., S. A. Foster, T. Keeling, K. G. Hubbard, C. Carlson, and R. Leeper, 2006: Impacts of irrigation on 20th century temperature in the northern Great Plains. *Global Planet. Change,* **54,** 1–18, doi:10.1016/j.gloplacha.2005.10.004.

Mapes, B. E., T. T. Warner, M. Xu, and D. J. Gochis, 2004: Comparison of cumulus parameterizations and entrainment using domain-mean wind divergence in a regional model. *J. Atmos. Sci.,* **61,** 1284–1295, doi:10.1175/1520-0469(2004)061<1284:COCPAE>2.0.CO;2.

McGuire, V. L., 2009: Water-level changes in the High Plains Aquifer, predevelopment to 2007, 2005–06, and 2006–07. Scientific Investigations Rep. 2009-5019, U.S. Geology Survey, Reston, VA, 15 pp.

Mellor, G. L., and T. Yamada, 1982: Development of a turbulence closure model for geophysical fluid problems. *Rev. Geophys.,* **20,** 851–875, doi:10.1029/RG020i004p00851.

Mesinger, F., and Coauthors, 2006: North American Regional Reanalysis. *Bull. Amer. Meteor. Soc.,* **87,** 343–360, doi:10.1175/BAMS-87-3-343.

Miguez-Macho, G., Y. Fan, C. P. Weaver, R. Walko, and A. Robock, 2007: Incorporating water table dynamics in climate modeling: 2. Formulation, validation, and soil moisture simulation. *J. Geophys. Res.,* **112,** D13108, doi:10.1029/2006JD008112.

Mlawer, E. J., S. J. Taubman, P. D. Brown, M. J. Iacono, and S. A. Clough, 1997: Radiative transfer for inhomogeneous atmospheres: RRTM, a validated correlated-k model for the longwave. *J. Geophys. Res.,* **102,** 16 663–16 682, doi:10.1029/97JD00237.

Moore, N., and S. Rojstaczer, 2001: Irrigation-induced rainfall and the Great Plains. *J. Appl. Meteor.,* **40,** 1297–1309, doi:10.1175/1520-0450(2001)040<1297:IIRATG>2.0.CO;2.

——, and ——, 2002: Irrigation's influence on precipitation: Texas High Plains, U.S.A. *Geophys. Res. Lett.,* **29,** doi:10.1029/2002GL014940.

Mu, Q., M. Zhao, and S. W. Running, 2011: Improvements to a MODIS global terrestrial evapotranspiration algorithm. *Remote Sens. Environ.,* **115,** 1781–1800, doi:10.1016/j.rse.2011.02.019.

NCAR Command Language, 2012: NCAR Command Language (version 6.2.0). Boulder, CO, UCAR/NCAR/CISL/VETS. [Available online at http://dx.doi.org/10.5065/D6WD3XH5.]

Niu, G.-Y., and Z.-L. Yang, 2004: The effects of canopy processes on snow surface energy and mass balances. *J. Geophys. Res.,* **109,** D23111, doi:10.1029/2004JD004884.

——, ——, R. E. Dickinson, and L. E. Gulden, 2005: A simple TOPMODEL-based runoff parameterization (SIMTOP) for use in global climate models. *J. Geophys. Res.,* **110,** D21106, doi:10.1029/2005JD006111.

——, ——, ——, ——, and H. Su, 2007: Development of a simple groundwater model for use in climate models and evaluation with Gravity Recovery and Climate Experiment data. *J. Geophys. Res.,* **112,** D07103, doi:10.1029/2006JD007522.

——, and Coauthors, 2011: The community Noah land surface model with multiparameterization options (Noah-MP): 1. Model description and evaluation with local-scale measurements. *J. Geophys. Res.,* **116,** D12109, doi:10.1029/2010JD015139.

Oleson, K. W., and Coauthors, 2010: Technical description of version 4.0 of the community land model (CLM). NCAR Tech. Note NCAR/TN-478+ STR, 257 pp.

Perkins, S. E., A. J. Pitman, N. J. Holbrook, and J. McAneney, 2007: Evaluation of the AR4 climate models' simulated daily maximum temperature, minimum temperature, and precipitation over Australia using probability density functions. *J. Climate,* **20,** 4356–4376, doi:10.1175/JCLI4253.1.

Qian, Y., M. Huang, B. Yang, and L. K. Berg, 2013: A modeling study of irrigation effects on surface fluxes and land–air–cloud interactions in the Southern Great Plains. *J. Hydrometeor.,* **14,** 700–721, doi:10.1175/JHM-D-12-0134.1.

Ruane, A. C., 2010: NARR's atmospheric water cycle components. Part II: Summertime mean and diurnal interactions. *J. Hydrometeor.,* **11,** 1220–1233, doi:10.1175/2010JHM1279.1.

——, and J. O. Roads, 2008: Diurnal to annual precipitation sensitivity to convective and land surface schemes. *Earth Interact.,* **12,** doi:10.1175/2008EI256.1.

Ruiz, J. J., C. Saulo, and J. Nogués-Paegle, 2010: WRF model sensitivity to choice of parameterization over South America: Validation against surface variables. *Mon. Wea. Rev.,* **138,** 3342–3355, doi:10.1175/2010MWR3358.1.

Saha, S., and Coauthors, 2010: The NCEP Climate Forecast System Reanalysis. *Bull. Amer. Meteor. Soc.,* **91,** 1015–1057, doi:10.1175/2010BAMS3001.1.

Santanello, J. A., M. A. Friedl, and M. B. Ek, 2007: Convective planetary boundary layer interactions with the land surface at diurnal time scales: Diagnostics and feedbacks. *J. Hydrometeor.,* **8,** 1082–1097, doi:10.1175/JHM614.1.

Schubert, S. D., M. J. Suarez, P. J. Pegion, R. D. Koster, and J. T. Bacmeister, 2008: Potential predictability of long-term drought and pluvial conditions in the U.S. Great Plains. *J. Climate,* **21,** 802–816, doi:10.1175/2007JCLI1741.1.

Skamarock, W. C., and Coauthors, 2008: A description of the Advanced Research WRF version 3. NCAR Tech. Note NCAR/TN-475+STR, 113 pp. [Available online at http://www.mmm.ucar.edu/wrf/users/docs/arw_v3_bw.pdf.]

Steeneveld, G. J., B. J. H. van de Wiel, and A. A. M. Holtslag, 2006: Modeling the evolution of the atmospheric boundary layer coupled to the land surface for three contrasting nights in CASES-99. *J. Atmos. Sci.,* **63,** 920–935, doi:10.1175/JAS3654.1.

Sun, Y., S. Solomon, A. Dai, and R. W. Portmann, 2007: How often will it rain? *J. Climate,* **20,** 4801–4818, doi:10.1175/JCLI4263.1.

Tuttle, J. D., and C. A. Davis, 2006: Corridors of warm season precipitation in the central United States. *Mon. Wea. Rev.,* **134,** 2297–2317, doi:10.1175/MWR3188.1.

Warrach, K., M. Stieglitz, H.-T. Mengelkamp, and E. Raschke, 2002: Advantages of a topographically controlled runoff simulation in a soil–vegetation–atmosphere transfer model. *J. Hydrometeor.,* **3,** 131–148, doi:10.1175/1525-7541(2002)003<0131:AOATCR>2.0.CO;2.

Weaver, S. J., and S. Nigam, 2008: Variability of the Great Plains low-level jet: Large-scale circulation context and hydroclimate impacts. *J. Climate,* **21,** 1532–1551, doi:10.1175/2007JCLI1586.1.

——, and ——, 2011: Recurrent supersynoptic evolution of the Great Plains low-level jet. *J. Climate,* **24,** 575–582, doi:10.1175/2010JCLI3445.1.

Wehner, M. F., R. L. Smith, G. Bala, and P. Duffy, 2010: The effect of horizontal resolution on simulation of very extreme United States precipitation events in a global atmosphere model. *Climate Dyn.,* **34,** 241–247, doi:10.1007/s00382-009-0656-y.

Whiteman, C. D., X. Bian, and S. Zhong, 1997: Low-level jet climatology from enhanced rawinsonde observations at a site in the Southern Great Plains. *J. Appl. Meteor.,* **36,** 1363–1376, doi:10.1175/1520-0450(1997)036<1363:LLJCFE>2.0.CO;2.

Xia, Y., and Coauthors, 2012: Continental-scale water and energy flux analysis and validation for the North American Land Data Assimilation System project phase 2 (NLDAS-2): 1. Intercomparison and application of model products. *J. Geophys. Res.,* **117,** D03109, doi:10.1029/2011JD016048.

——, and Coauthors, 2013: Validation of Noah-simulated soil temperature in the North American Land Data Assimilation System Phase 2. *J. Appl. Meteor. Climatol.,* **52,** 455–471, doi:10.1175/JAMC-D-12-033.1.

Xie, Z., Z. Di, Z. Luo, and Q. Ma, 2012: A quasi-three-dimensional variably saturated groundwater flow model for climate modeling. *J. Hydrometeor.,* **13,** 27–46, doi:10.1175/JHM-D-10-05019.1.

Yang, R., and M. A. Friedl, 2003: Modeling the effects of 3-D vegetation structure on surface radiation and energy balance in boreal forests. *J. Geophys. Res.,* **108,** 8615, doi:10.1029/2002JD003109.

Yang, Z.-L., and G.-Y. Niu, 2003: The versatile integrator of surface and atmosphere processes: Part 1. Model description. *Global Planet. Change,* **38,** 175–189, doi:10.1016/S0921-8181(03)00028-6.

——, and Coauthors, 2011: The community Noah land surface model with multiparameterization options (Noah-MP): 2. Evaluation over global river basins. *J. Geophys. Res.,* **116,** D12110, doi:10.1029/2010JD015140.

Yuan, H., R. E. Dickinson, Y. Dai, M. J. Shaikh, L. Zhou, W. Shangguan, and D. Ji, 2014: A 3D canopy radiative transfer model for global climate modeling: Description, validation, and application. *J. Climate,* **27,** 1168–1192, doi:10.1175/JCLI-D-13-00155.1.

Zhang, G. J., and N. A. McFarlane, 1995: Sensitivity of climate simulations to the parameterization of cumulus convection in the Canadian Climate Centre general circulation model. *Atmos.–Ocean,* **33,** 407–446, doi:10.1080/07055900.1995.9649539.

Zhang, Y., and S. A. Klein, 2010: Mechanisms affecting the transition from shallow to deep convection over land: Inferences from observations of the diurnal cycle collected at the ARM Southern Great Plains site. *J. Atmos. Sci.,* **67,** 2943–2959, doi:10.1175/2010JAS3366.1.

Zhong, S., and J. C. Doran, 1995: A modeling study of the effects of inhomogeneous surface fluxes on boundary-layer properties. *J. Atmos. Sci.,* **52,** 3129–3142, doi:10.1175/1520-0469(1995)052<3129:AMSOTE>2.0.CO;2.

——, and ——, 1997: A study of the effects of spatially varying fluxes on cloud formation and boundary layer properties using data from the Southern Great Plains Cloud and Radiation Testbed. *J. Climate,* **10,** 327–341, doi:10.1175/1520-0442(1997)010<0327:ASOTEO>2.0.CO;2.

——, J. D. Fast, and X. Bian, 1996: A case study of the Great Plains low-level jet using wind profiler network data and a high-resolution mesoscale model. *Mon. Wea. Rev.,* **124,** 785–806, doi:10.1175/1520-0493(1996)124<0785:ACSOTG>2.0.CO;2.

Zhu, J., and X.-Z. Liang, 2007: Regional climate model simulations of U.S. precipitation and surface air temperature during 1982–2002: Interannual variation. *J. Climate,* **20,** 218–232, doi:10.1175/JCLI4129.1.